2023

MIXING, METABOLISM, AND CLIMATE CHANGE: A MODELING CASE STUDY OF A SHALLOW HYPEREUTROPHIC, POLYMICTIC LAKE

Benjamin C. Reuss
Michigan Technological University, bcreuss@mtu.edu

MIXING, METABOLISM, AND CLIMATE CHANGE: A MODELING CASE STUDY OF A SHALLOW HYPEREUTROPHIC, POLYMICTIC LAKE

By

Benjamin C. Reuss

A THESIS

Submitted in partial fulfillment of the requirements for the degree of

MASTER OF SCIENCE

In Environmental Engineering

MICHIGAN TECHNOLOGICAL UNIVERSITY

2023

This thesis has been approved in partial fulfillment of the requirements for the Degree of MASTER OF SCIENCE in Environmental Engineering.

Department of Civil, Environmental, and Geospatial Engineering

Thesis Advisor:	*Dr. Noel Urban*
Committee Member:	*Dr. Cory McDonald*
Committee Member:	*Dr. Amy Marcarelli*
Department Chair:	*Dr. Audra Morse*

Table of Contents

List of Figures v

List of Tables vi

Author Contribution Statement vii

Acknowledgements viii

Abstract ix

1 Lake Mixing Dynamics 1

2 Effect of Mixing on Ecosystem Metabolism in a Shallow, Hypereutrophic, Polymictic Lake 8
- 2.1 Background 8
- 2.2 Methods 12
  - 2.2.1 Study Site 12
  - 2.2.2 Data Collection 13
  - 2.2.3 Data Analysis 14
- 2.3 Results 17
- 2.4 Discussion 21
- 2.5 Conclusions 25

3 Effects of Climate Change on Hydrodynamics in a Shallow, Hypereutrophic, Polymictic Lake 26
- 3.1 Background 26
- 3.2 Methods 31
  - 3.2.1 Study Site 31
  - 3.2.2 Field Methods and Data Acquisition 31
  - 3.2.3 Model Description 32
  - 3.2.4 Model Calibration 33
  - 3.2.5 Model Application 35
  - 3.2.6 Climactic Inputs 37
- 3.3 Results 38
- 3.4 Discussion 44
- 3.5 Conclusions 49

4 References 50

5 Appendix 55
- 5.1 Goose Lake 55
- 5.2 Metabolism Modeling 57
- 5.3 GLM Modeling 59

5.3.1 GLM Configuration File 59
5.4 R Code 63
5.4.1 Calibration Setup 63
5.4.2 Simulated Annealing Calibration 64
5.4.3 Simulated Annealing Call 66
5.4.4 2019 Mixing Analysis 67
5.4.5 Future Scenario Mixing Analysis 70

List of Figures

Figure 2.1. Goose Lake, Marquette Co. MI USA 12
Figure 2.2. Goose Lake 2019 Temperature Profile 17
Figure 2.3. Productivity Timeseries of Daily NEP, GPP, R and F. 18
Figure 3.1. 2019 Modeled Temperature Profile 39
Figure 3.2. Future Model Temperature Profile. 41
Figure 3.3. Stratification Extent Sensitivity Analysis 43
Figure 5.1. Goose Lake Hypsographic Curve 55
Figure 5.2. Observed 2019 DO Profile 56

List of Tables

Table 2.1. Average Monthly Productivity (g O2 m-3 d-1) 18
Table 2.2. dLNdt-1 and dProductivitydt-1 Cross-Correlations 19
Table 2.3. Light, Mixing Depth, and Epilimnion Temperature Spearman Correlations ... 20
Table 2.4. Measured 2019 DOC Concentrations (mg/L) 20
Table 3.1. Study Period Climate Averages 37
Table 3.2. GLM Calibrated Parameters 38
Table 3.3. Change in Climate Drivers Relative to 2019 39
Table 3.4. Future Scenario Analyses 42
Table 5.1. Pearson and Cross-Correlation Comparison 58
Table 5.2. GLM Sensitivity Analysis Results 62

Author Contribution Statement

Benjamin Reuss assisted with the study design and conducted the data analysis, manuscript drafting, and manuscript review. Dr. Cory McDonald assisted with the study design, data interpretation, manuscript review and oversaw fieldwork. Dr. Noel Urban assisted with data interpretation and manuscript review.

Acknowledgements

The Civil, Environmental, and Geospatial Engineering Department at Michigan Technological University provided funding for this work. The Great Lakes Research Center provided partial funding support for the hydrodynamic modeling chapter. The authors would like to thank Kenny Larsen and Mahta Naziri-Saeed for collecting the field data.

Abstract

Globally, lakes are sites of significant carbon cycling, respiring an estimated 0.07 to 0.15 Pg as CO_2 and sequestering 0.03 to 0.07 Pg C in sediments annually. These processes can be affected by nutrient availability, with seasonal mixing regulating nutrient transport in monomictic and dimictic systems. However, the effect of intermittent mixing on ecosystem production in polymictic systems has been much less studied. The timing and frequency of lake mixing are expected to be altered by climate change, which has the potential to impact nutrient transport. The first chapter of this thesis introduces lake mixing dynamics and indices of mixing. In chapter two, the relationship between intermittent mixing and changes in productivity in polymictic systems is examined, under the hypothesis that productivity will increase in response to lake mixing. Ecosystem productivity was calculated via the diel oxygen technique for Goose Lake, Marquette Co., MI, over the 2019 field season. The diel changes in Net Ecosystem Production (NEP), Gross Primary Production (GPP), and Respiration (R) were cross-correlated with the diel change in Lake Number (LN), an index of stratification. One day after mixing, dNEP dt^{-1} and dGPP dt^{-1} were negatively correlated with dLN dt^{-1} with coefficients of -0.342 and -0.209, respectively, at a cross correlation significance threshold of ±0.1859. This corresponds to an increase in NEP and GPP as LN decreases. These correlations suggest that GPP and NEP increase in response to mixing. In chapter three, climate-driven changes in stratification extent and mixing frequency are modeled for the early 2080's relative to 2019. The one-dimensional General Lake Model (GLM) was autocalibrated for 2019 conditions using simulated annealing. The cost function consisted of the sum of temperature and Lake Number Normalized Root Mean Squared Error (NRMSE) to

improve vertical heat distribution. Six Coupled Model Intercomparison Project 5 (CMIP5) climate models for the early 2080's were input into the GLM model to determine changes in hydrodynamics. In all future scenarios, stratification extent and water temperatures increased relative to 2019. However, mixing frequency also increased and the lake remained polymictic. This increase in stratification is likely due to both increased air temperatures and lower wind speeds. Increased stratification and temperatures will likely exacerbate existing water quality problems by stimulating DO drawdowns and internal loading of phosphorus. These conditions will increase the probability of cyanobacteria blooms. Higher temperatures will likely shift the system further towards net heterotrophy due to the greater temperature dependence of respiration than photosynthesis. While the number of mixing events increased, this was due to significantly increased stratification which would be expected to decrease productivity. Therefore, it cannot be conclusively determined if productivity will increase in Goose Lake in response to climate change.

1 Lake Mixing Dynamics

Vertical mixing in lakes is a phenomenon that regulates many other processes, such as nutrient and dissolved oxygen (DO) transport, that in turn affect lake metabolism (Nürnberg 1998; Wilhelm and Adrian 2008; Fukushima et al. 2019; Cortés et al. 2021). Lakes mix when external forces overcome water column inertia, inducing mixing (Robertson and Imberger 1994). Climate change is contributing to a general decrease in mixing frequency by altering the drivers of mixing and stability (Kirillin 2010; Woolway et al. 2017; Woolway and Merchant 2019). However, some small lakes have been modeled as increasing in mixing frequency due to increased wind speeds (Woolway and Merchant 2019). This section will briefly introduce lake mixing and provide a roadmap for future chapters.

Lakes stratify due to vertical thermal or chemical density gradients within the water column (Boehrer and Schultze 2008). These gradients can produce defined layers; the least dense surface layer, or epilimnion, sits atop the denser hypolimnion. The two layers are separated by the metalimnion, a zone of temperature change that contains the thermocline, the layer of the largest temperature gradient. Molecular transport is inhibited across the thermocline (Boehrer and Schultze 2008). This separation can cause the isolated hypolimnion to experience hypoxia due to DO drawdowns (Fukushima et al. 2019; Cortés et al. 2021). Hypoxia can exacerbate the release of phosphorus bound in sediments due to changing redox conditions (Sondergaard et al. 2001). This phenomenon, known as internal loading, is a water quality concern in many lakes. A major mechanism to resupply hypolimnetic oxygen is vertical mixing from surface waters that are in contact with the atmosphere (Robertson and Imberger 1994; Fukushima et al. 2019). Nutrient-rich water

from the hypolimnion can increase productivity when mixed into the photic zone (Wilhelm and Adrian 2008).

The breakdown of thermal gradients by external forces results in mixing. These forces primarily include wind but can result from gains or losses of lake water or changing density (Robertson and Imberger 1994; Boehrer and Schultze 2008). The latter is not limited to warming because water has a maximum density at 4 °C. In temperate regions, this can cause inverse stratification during the winter ice period, where water is coldest near the surface ice and warmest near the lakebed (Woolway et al. 2020). When the surface warms in the spring, the former ice is warmed to 4 °C and sinks, inducing mixing.

The thermal gradients themselves are controlled by a myriad of processes that comprise a lake's heat budget. Warming effects include shortwave radiation from the sun and longwave radiation from the atmosphere (Woolway et al. 2020; Schmid and Read 2022). Cooling effects include evaporation and longwave radiation emitted by the lake. Other processes can have variable temperature effects on the lake, such as thermal conduction to and from the atmosphere (sensible heat), sediment heating, groundwater intrusion, inflowing water from surface sources, and precipitation.

Shortwave radiation directly warms lakes (Woolway et al. 2020; Schmid and Read 2022). Some shortwave radiation is reflected at the surface, but the remainder is attenuated within the water column (Boehrer and Schultze 2008). The surface reflectivity, or albedo, is especially high during the ice-covered season. Decreased ice cover has a warming effect on the lake because increased sunlight can enter the water column (Woolway et al. 2020).

However, warming is somewhat counteracted through increased evaporation and sensible heat loss (Zhong et al. 2016).

The behavior of shortwave radiation is heavily influenced by the transparency of the water. (Rose et al. 2016; Pilla et al. 2018) In clear waters, sunlight can penetrate deep into the water column. In turbid lakes, shortwave radiation is rapidly attenuated near the surface, which can strengthen stratification by warming surface waters. Due to this behavior, changing water clarity can profoundly impact lake warming and mixing dynamics (Kirillin 2010; Rose et al. 2016; Pilla et al. 2018).

Longwave radiation is emitted by both the atmosphere and the lake surface (Hipsey et al. 2019; Woolway et al. 2020; Schmid and Read 2022). Both fluxes depend on temperature, but atmospheric longwave radiation is also affected by cloud cover, humidity, and albedo at the water's surface. These two forces can have competing effects on lake warming. If warmer air temperatures increase downwelling longwave radiation, which warms the water's surface, outgoing radiation and evaporation will both increase, providing a cooling effect (Woolway et al. 2020)

In addition to changing the water budget of a lake, evaporation is an important cooling process. The phase change from liquid to gas requires energy, known as latent heat, which cools the lake. Evaporation is regulated by water temperature, humidity, and wind speed (Boehrer and Schultze 2008; Hipsey et al. 2019; Schmid and Read 2022). Condensation has a warming effect, but the effect on the heat budget is small relative to evaporation.

Sensible heat and inflowing water can have variable impacts on the heat budget. The direction of sensible heat transfer between the lake surface and the atmosphere depends on the relative temperature difference between the two. However, according to Schmid and Read (2022), the net effect tends to be cooling. Surface water inflows, precipitation, or groundwater intrusion affect the heat budget based on their relative temperature. However, the temperature and location of the inflows can alter water column stability (Hipsey et al. 2019; Schmid and Read 2022). Cold river water can "plunge" to the hypolimnion and strengthen stratification, whereas warm groundwater intrusion can destabilize the hypolimnion. The sediment can warm or cool the hypolimnion based on the relative temperature difference.

One method of classifying lakes is by mixing frequency. Common in temperate regions, dimictic lakes mix twice per year, typically in spring and fall (Boehrer and Schultze 2008; Woolway et al. 2020). Monomictic lakes mix once per year, whereas amictic lakes are stratified year-round. Polymictic lakes mix multiple times per year and are subdivided into continuous lakes, which are consistently well-mixed, and discontinuous lakes that experience periodic stratification. Polymictic lakes are typically shallow because less water mass makes it easier for mixing to occur.

There are several uncertainties in the response of small lakes to climate change. Mixing frequency in polymictic lakes is especially sensitive to wind forcing (Woolway et al. 2017). While lakes are generally expected to mix less frequently due to climate change, some modeling studies showed increases in mixing frequencies due to heightened wind speeds (Woolway and Merchant 2019). Other studies have found that changes in

transparency are the main regulator of the climactic response in polymictic lakes (Kirillin 2010). Because mixing affects nutrient transport, changing mixing dynamics can affect productivity (O'Reilly et al. 2003). This thesis will focus on the drivers and impacts of mixing in polymictic lakes.

There are many methods to quantify stratification and mixing in lakes, ranging in complexity from a simple 1 °C temperature gradient per meter to complex calculations of inertia. Schmidt Stability and Lake Number (LN) will be discussed here. Lake Number will be used extensively in the following chapters to quantify mixing and identify stratified periods.

Schmidt Stability was proposed as a metric of the amount of work that is required to mix a body of water to a uniform density (Idso 1973). This metric is impacted by lake morphology and size, so it was refined to be calculated on a normalized basis. The equation used by Robertson and Imberger (1994) is as follows:

$$S_t = 1/A_m \int_0^{Z_m} (z - Z_g) * A_z * (1 - \rho_z) * dz$$

[1.1] (Robertson and Imberger 1994)

Where z is the height from the lakebed in cm, A_m and A_z are the lake surface and z–height areas in cm^2, Z_m and Z_g are the maximum lake depth and height of the center of gravity above the lakebed, and ρ_z is the water density at height z in g cm^{-3}. The units for S_t are g cm cm^{-2}. One limitation of Schmidt Stability noted by Robertson and Imberger (1994) is that even if S_t is low, it does not necessarily mean that mixing will occur if external wind

forcing is also low. They built on S_t to develop Lake Number, which considered wind conditions to measure the potential for mixing.

Lake Number is a unitless index that measures water column stability about the lake's center of gravity (Robertson and Imberger 1994). The index compares the amount of energy required to mix the lake, calculated using Schmidt Stability, with the actual energy provided by wind forcing. In this calculation, wind is assumed to be the dominant mixing force acting on the lake (Robertson and Imberger 1994). A value of LN >1 indicates stratified conditions, while LN <1 indicates potential for mixing. The modified equation developed by Robertson and Imberger (1994) is as follows:

$$L_N = \frac{g * S_t * \left(1 - \frac{Z_t}{Z_m}\right)}{(\rho_m * u_*^2 * A_m^{1.5} * (1 - \frac{Z_g}{Z_m}))} \quad [1.2]$$

Where g is gravity in cm s^{-2}, Z_t is thermocline height in cm, ρ_m is water density at the surface and, A_m is lake surface area in cm^2. The water-friction velocity is defined as:

$$u_*^2 = \frac{\rho_a}{\rho_m} * C_D * U_{10}^2 \quad [1.3]$$

Where ρ_a is air density, Cd is the drag coefficient, and U_{10} is the wind speed 10 meters above the lake in cm s^{-1}. In subsequent chapters, LN will be used as a quantitative measure of mixing and stratification.

The second chapter of this thesis examines the impact of mixing on metabolism in temperate, polymictic, hypereutrophic Goose Lake. Lake metabolism is first quantified for the 2019 field season using the diel oxygen technique (Staehr et al. 2010). Next, the

changes in productivity and Lake Number were cross-correlated to examine delayed signals between mixing events and productivity. Mechanistically, mixing should stimulate nutrient transport into the photic zone, which would increase productivity. A study by Wilhelm and Adrian (2008) found increases in algal biomass after recovery from long periods of stratification in polymictic lake Müggelsee, which they attributed to increased nutrient transport. We hypothesize that productivity will increase in response to mixing in Goose Lake.

In the final chapter, the impact of climate change on lake hydrodynamics is explored. While mixing frequencies are generally expected to decrease due to warming, some modeling studies have shown increasing frequencies in shallow lakes due to greater wind forcing (Woolway et al. 2017, 2019; Woolway and Merchant 2019). Kirillin (2010) modeled regime shifts from polymictic to monomictic in Lake Müggelsee by the end of the century and predicted similar outcomes for other temperate, polymictic lakes.

To examine potential changes to mixing, a one-dimensional hydrodynamic model of Goose Lake was constructed using the General Lake Model (Hipsey et al. 2019). The model was autocalibrated via simulated annealing to the observed 2019 season (Xiang et al. 2013). Six future climate models from the CMIP5 dataset were used as inputs to determine future hydrodynamics (Taylor et al. 2012). Finally, a sensitivity analysis was conducted for windspeed, transparency, and inflow conditions. The objectives of this chapter are to determine potential alterations in mixing frequency in response to climate change and to explore model sensitivity to wind speed and transparency, both defined as critical parameters in other studies (Kirillin 2010; Woolway et al. 2017; Pilla et al. 2018).

2 Effect of Mixing on Ecosystem Metabolism in a Shallow, Hypereutrophic, Polymictic Lake

2.1 Background

Lakes are sites of significant carbon cycling. Globally, lakes respire an estimated 0.07 to 0.15 Pg C as CO2 and sequester 0.03 to 0.07 Pg in sediments on an annual basis (Cole et al. 2007). A lake receives carbon inputs from the watershed as Dissolved Organic Carbon (DOC), Particulate Organic Carbon, and Dissolved Inorganic Carbon in addition to atmospheric CO2 fluxes (Tranvik et al. 2009). Carbon is fixed into biomass by primary producers and respired by both primary producers and heterotrophs. Both organic and inorganic carbon can settle to the lakebed and be sequestered in sediments (Tranvik et al. 2009). Carbon is also exported downstream, though the importance of this process varies depending on the system. Biological activity is a significant driver of carbon cycling in lakes (Tranvik et al. 2009; Cortés et al. 2021).

A method of quantifying the biologic carbon processing of a system is through the lens of ecosystem metabolism. In lakes, the diel oxygen technique is most commonly used due to ease of instrument deployment and relatively low costs compared to bottle incubations (Staehr et al. 2010). This method derives ecosystem metabolism from high temporal resolution Dissolved Oxygen (DO) data. As photosynthesis and aerobic respiration involve both carbon and oxygen, a mass balance for either element enables the calculation of metabolism (Laas et al. 2012). The diel oxygen technique directly yields Net Ecosystem Production (NEP), which is further broken down into Gross Primary Production (GPP) and Respiration (R).

Gross Primary Production is the rate of oxygen production by photosynthesis, whereas R is the rate of oxygen consumption by aerobic respiration (Staehr et al. 2010). Net Ecosystem Production is the difference between the two. A positive NEP (GPP > R) indicates net autotrophy, where the system accumulates more carbon in biomass than is respired. A negative NEP indicates net heterotrophy, where the system releases more carbon into the atmosphere than it fixes into biomass. Even highly productive lakes can be net heterotrophic due to external carbon inputs from the watershed (Prarie and Bird 2002). A study of 33 Quebec lakes modeled a shift to net heterotrophy at epilimnetic DOC concentrations > 5 mg L^{-1} (Prarie and Bird 2002). However, the carbon balance in lakes can be seasonal, with net heterotrophic and net autotrophic regimes present at different times of the year (Staehr and Sand-Jensen 2007; Laas et al. 2012).

Lovett et al. (2006) note that a positive NEP is not always synonymous with carbon sequestration, but is the total amount of carbon available for transport, sequestration, or loss from the system by other means (e.g., macrophyte harvesting). Notably, in addition to burial in sediments, significant quantities of carbon can be exported downstream. While not a complete predictor of the fate of carbon, NEP is still a valuable tool for understanding the ecosystem dynamics of a lake.

Lakes are classified by their mixing frequency; monomictic, dimictic, and polymictic lakes mix once, twice, or multiple times per year, respectively. Lake mixing is a critical process that regulates oxygen and nutrient concentrations throughout the water column (Fukushima et al. 2019; Cortés et al. 2021). Lakes stratify due to temperature-induced density gradients. These gradients can be disrupted by wind energy or increasing

density of upper layers, resulting in vertical mixing. The latter can be due to heating or cooling because water has a maximum density at 4℃.

These mixing processes move oxygen-rich water to lower depths and nutrient-rich water into the photic zone (Cortés et al. 2021). In dimictic lakes, this overturn occurs twice per year, in the spring and fall, and the increased available nutrients are then utilized by microbes and macroscopic plants (Nürnberg 1998). It is unclear if productivity increases due to periodic mixing in polymictic systems. The shorter periods of stratification may not lead to significant DO drawdowns in the hypolimnion, which could stymie redox-driven internal loading of phosphorus (Cortés et al. 2021). However, significant oxygen demand has been observed before DO drawdowns in polymictic lakes (Fukushima et al. 2019).

In addition to nutrient limitation, the growth of phytoplankton can also be limited by light availability (Torremorell et al. 2009; Staehr et al. 2016). While algae need light to photosynthesize, excess light can reduce productivity via photoinhibition. Plankton biomass can also create feedback loops of light limitation, where high concentrations can decrease water clarity, ultimately decreasing productivity. Photoinhibition is more common in oligotrophic, nutrient poor systems while light limitation is more common in nutrient rich, turbid systems (Staehr et al. 2016).

Climate change is expected to impact the timing and frequency of lake mixing (Butcher et al. 2015; Woolway et al. 2017; Woolway and Merchant 2019). Higher air temperatures will shift the onset of stratification to earlier in the season and strengthen vertical thermal gradients. The duration of stratification also increases due to warmer temperatures persisting later into fall. Increased duration and strength of stratification may

exacerbate hypoxia, which in turn can lead to increased internal phosphorus loading or fish kills (Cortés et al. 2021). Altered wind speeds associated with climate change can also affect the depth, stability, and duration of stratification (Woolway et al. 2017; Woolway and Merchant 2019).

Due to the connection between mixing and nutrient transport, changes to mixing frequency in polymictic systems could directly impact lake metabolism. While this relation is well documented in lakes that mix seasonally, there is a lack of research in polymictic systems (Nürnberg 1998; Cortés et al. 2021). A study by Wilhelm and Adrian (2008) found evidence of increased phytoplankton biomass following mixing events in polymictic Lake Müggelsee in Germany, which they attributed to the internal loading of phosphorus. While that study included a detailed analysis of plankton communities and water chemistry after long periods of stratification, they did not calculate rapid changes in ecosystem metabolism due to short-term stratification and mixing events.

This chapter aims to examine the relationship between intermittent mixing and changes in productivity in polymictic systems. We hypothesize that productivity will increase in response to mixing in polymictic lakes. This paper will present a case study of productivity and mixing dynamics of Goose Lake, a shallow, hypereutrophic, polymictic lake in the Great Lakes Region.

2.2 Methods

2.2.1 Study Site

Goose Lake, in Marquette Co., MI, is a small, shallow, polymictic lake in the Great Lakes region, shown in Figure 2.1. The lake is listed on the state's Clean Water Act 303(d) list as impaired for phosphorus due to historical wastewater discharge from the nearby town of Negaunee (White Water Associates 2003; Holden 2011). Phosphorus concentrations remain elevated primarily due to internal loading (Holden 2011).

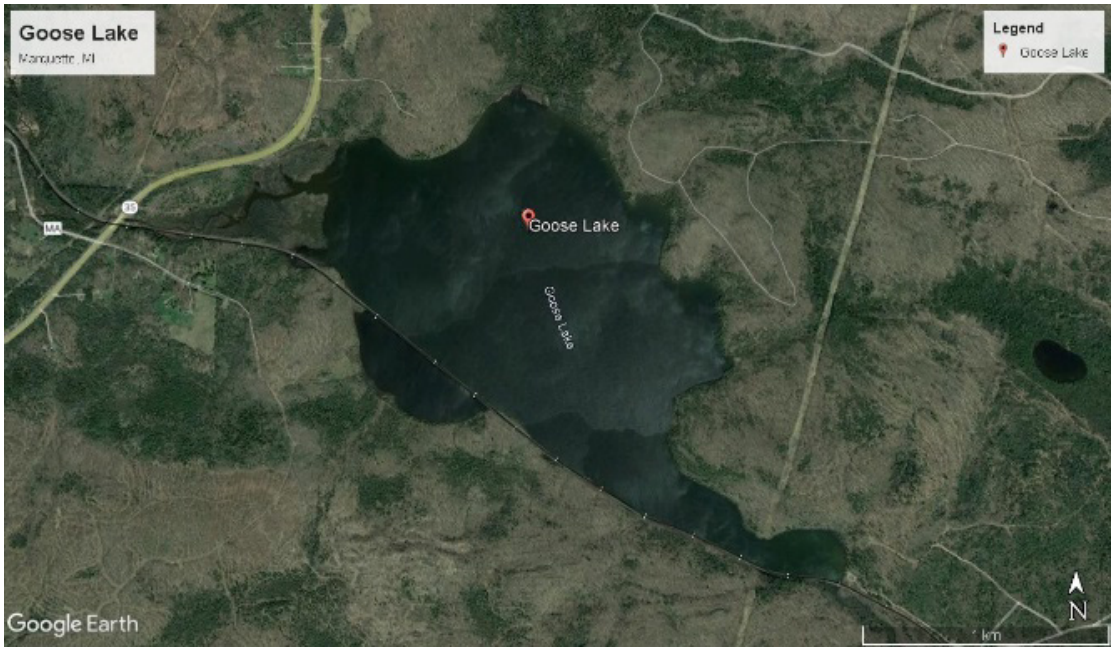

Figure 2.1. Goose Lake, Marquette Co. MI USA

The railroad bridge is visible in the southeastern basin of the lake.

Goose Lake has a surface area of 1.74 km^2, maximum depth of 4.57 m, and hydraulic retention time of 0.56 years (Holden 2011; 2021). A railroad line bisects the lake in the southwestern portion. The smaller section was assumed to have low connectivity and was excluded from the analysis, yielding a remaining lake area of 1.69 km^2.

The watershed is 37.7 km^2 and consists of 77% natural, 15% barren, and 8% urban land uses (Purdue University 2021). For the natural land use, 11% of the total watershed area is wetlands and 66% is forested. The barren region is a result of iron mining activity (Holden 2011). The primary hydrologic input is Partridge Creek, though several small, unnamed streams are also present (White Water Associates 2003; Holden 2011). Few macrophytes were observed during the study period.

2.2.2 Data Collection

A NexSens CB-450 buoy was deployed for 134 days from June to October 2019 at the deepest point in the lake (4.57 m). Attached to the buoy was a chain of NexSens thermistors from 0.5 to 4.5 m depth at 0.5-m intervals and HOBO Dissolved Oxygen Data Loggers at 2, and 4 m. A YSI EXO2 sonde at 1-m depth monitored temperature and DO. An AIRMAR WeatherStation 200 WX on the buoy measured wind at 1-m height in addition to air temperature, and pressure. Shortwave radiation was recorded using a LICOR pyranometer. All sensors sampled at 10-min intervals, though 24-hour data gaps at the end of each month were present. Gaps in the recorded windspeed and water temperature data were filled by repeating the previous day's observations. These periods were between 4:00 pm and 11:50 pm on the last day of each month and midnight to 3:50 pm on the first day of each month.

Water samples were collected at 0-, 2-, and 4-m depths at the buoy on seven days throughout the study period. The sampling interval was variable, starting at two-week intervals from 5/23 to 7/2 and subsequently being measured on 7/25, 8/29, and 10/24. Dissolved organic carbon was only collected on the first 4 sample dates of 5/23, 6/7, 6/19,

and 7/2. Phosphorus concentrations were analyzed via the ascorbic acid method, while DOC was analyzed using a Shimadzu TOC analyzer.

Bathymetry and productivity calculations were completed in Excel, whereas calculation of lake indices and statistical analyses were conducted in R (R Core Team 2022). Lake bathymetry was derived from a Navionics bathymetry map (2021). This map was traced in an image processor to calculate the total number of pixels corresponding to each contour. The pixels were converted to square meters by scaling to the total lake area delineated in Google Earth Pro.

2.2.3 Data Analysis

The methods of Staehr et al. (2010) were used to calculate ecosystem metabolism via the diel oxygen technique. The governing equation is as follows:

$$NEP = GPP - R - F - A \qquad [2.1] \text{ (Staehr et al. 2010)}$$

Where F is atmospheric flux. A includes all other processes, such as advection, and is typically neglected. Net Ecosystem Production is calculated for each timestep via equation 2.2, where F is atmospheric flux and Z is the depth of the mixed layer. NEP is in units of $gO_2m^{-3}10\ min^{-1}$. Atmospheric flux is positive when the lake is supersaturated with oxygen and emits oxygen to the atmosphere and is defined in equation 2.3. Flux is in units of $gO_2m^{-2}10\ min^{-1}$and k is piston velocity.

$$NEP_{10} = \Delta O_2 - F/Z_{mix} \qquad [2.2]$$

$$F_{10} = k(O_{2meas} - O_{2sat}) \qquad [2.3]$$

The mean rate of respiration over the entire day is assumed to be equivalent to the mean NEP during darkness. Daylight was defined as intervals > 40 W m^{-2} of incident shortwave radiation, consistent with Turan and Karakaya (2017).

Due to the polymictic nature of the lake, several assumptions were made in the analysis that slightly deviated from the established methods. The 1-m DO sensor was assumed to be representative of the mixed layer DO concentration. This sensor was deployed the earliest in the season and should always be contained within the mixed layer. When the lake was mixed, lower depths had equivalent DO concentrations, shown in Figure 5.1. Dissolved oxygen saturation was obtained directly from the sensor and not calculated using the formulas from Staehr et al. (2010).

Lake Number was used as a measure of stratification and mixing events (Robertson and Imberger 1994). This index utilizes the Schmidt Stability to balance water column density gradients and wind forcing to determine the mixing behavior of a lake (Robertson and Imberger 1994). An LN > 1 indicates stratification while LN < 1 indicates mixed conditions.

This Lake Number timeseries was calculated using the Lake Analyzer package in R using a 1-hour time step that was then averaged to a daily interval. Lake Analyzer is an R package that can calculate parameters and indices from observed environmental datasets (Read et al. 2011). The minimum metalimnion temperature gradient, used in calculating LN, was set to zero to allow for a continuous calculation. Lake Number was sometimes calculated as a slightly negative value during unstratified periods when the lake was completely mixed. These values were replaced with zero since complete mixing was

assumed. This 60-min data was averaged to a daily interval for use in the correlation analysis. Because the diel oxygen technique inherently uses a diel timestep, all other parameters were calculated as average daily values to allow for comparison. Average mixing depth and volumetrically averaged epilimnion temperatures were also calculated from the bathymetry and thermistor data using Lake Analyzer.

Cross-correlations were calculated between daily dLN dt^{-1} and dProductivity dt^{-1} to examine the relationship between mixing and productivity (R Core Team 2022). This analytical method was selected because we expected to see a delayed response as the phytoplankton utilized increased nutrients. The underlying calculation is a Pearson correlation on the lagged data. Thresholds of significance are based on the number of samples included in the appendix. A time lag of ± 5 days was chosen to analyze short-term mixing. This cross-correlation cannot contain negative values, so a flat integer was added to each parameter. In addition, Spearman correlations were determined between average irradiance, water temperature, mixing depth, and productivity metrics for each day, because light and temperature are expected to influence metabolic processes (Yvon-Durocher et al. 2010; Harrell Jr. 2022).

2.3 Results

The temperature profile for Goose Lake during the study period is shown in Figure 2.2. Multiple stratification and mixing events are evident, particularly during July and August. The highest daily average epilimnion temperature of 25.11 °C occurred on July 20th. The first temperature sensor was located at a 0.5-m depth, so the upper portion of the profile has been omitted. A timeseries of DO concentrations is supplied in the appendix.

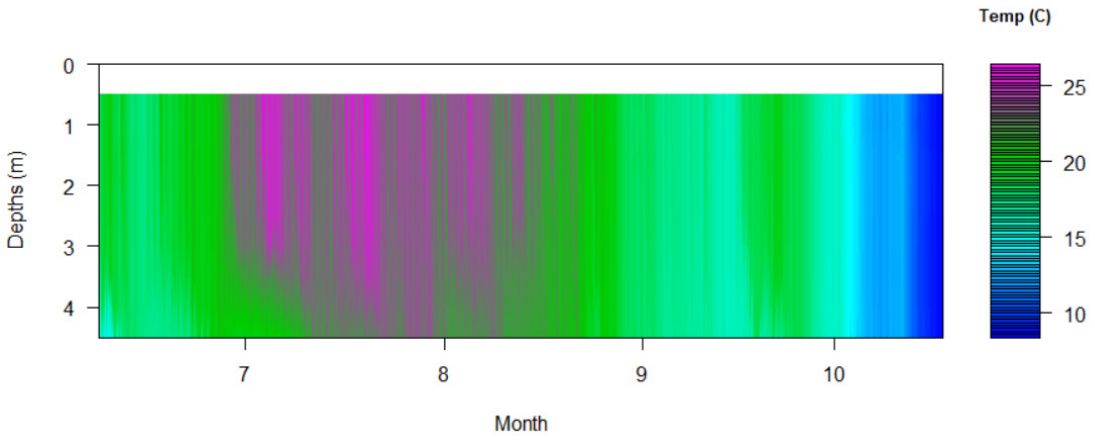

Figure 2.2. Goose Lake 2019 Temperature Profile.

The plot interpolates the thermistors at 0.5 m intervals from 0.5 to 4.5 m. Deployment dates spanned 6/7 to 10/18 2019.

Figure 2.3 displays the times series of calculated NEP, GPP, and R for the study period, while Table 2.1 includes monthly averages. October 15th - 18th were omitted from the analyses because a positive respiration value was calculated for each day. In the plot, respiration is signified as a negative value.

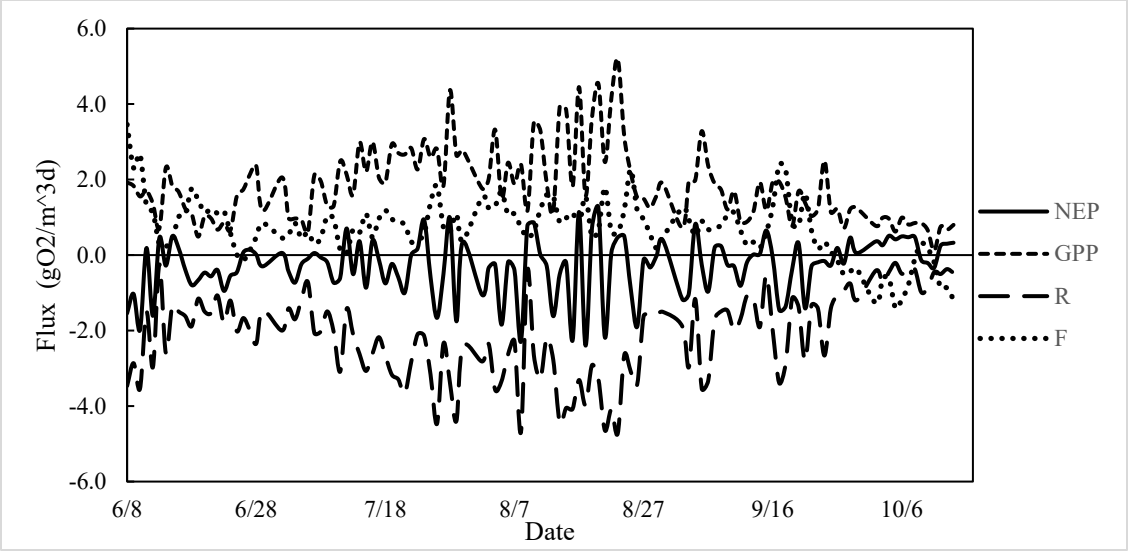

Figure 2.3. Productivity Timeseries of Daily NEP, GPP, R and F.

Respiration is denoted as a negative value. Negative NEP values denote periods of net heterotrophy and positive values net autotrophy. The first and last days of each month were omitted.

Table 2.1. Average Monthly Productivity (g O2 m-3 d-1)

Month	R	GPP	NEP	F
Jun	1.876	1.402	-0.474	1.076
Jul	2.474	2.212	-0.263	0.717
Aug	3.033	2.588	-0.445	1.049
Sept	1.794	1.515	-0.280	0.681
Oct	0.511	0.757	0.246	-0.738

All productivity metrics are in (g O_2 m^{-3} d^{-1}). Flux is in (g O_2 m^{-2} d^{-1}). The highest magnitude of GPP and R occurred in July and August. October was the only month with a positive NEP.

All months other than October had a negative NEP. This indicates a switch from net heterotrophy to net autotrophy at the end of the season. The highest magnitudes of R (3.033 g O_2 m^{-3} d^{-1}) and GPP (2.588 g O_2 m^{-3} d^{-1}) both occurred in August, with the lowest magnitudes occurring in October. Flux was positive for all months except October.

The results of the cross-correlation analysis between dLN dt^{-1} and dProductivity dt^{-1} are shown in Table 2.2. One day after mixing (Lag = -1), dNEP dt^{-1} and dGPP dt^{-1} were negatively correlated with dLN dt^{-1} with coefficients of -0.342 and -0.209, respectively. This corresponds to an increase in NEP and GPP as LN decreases. On the day of mixing (Lag = 0) dNEP dt^{-1} was positively correlated, and dR dt^{-1} was negatively correlated with dLN dt^{-1} at 0.225 and -0.202 respectively. As Lake Number decreases, the magnitude of R increases. This increase lowers the value of NEP, resulting in a positive correlation. The cross correlation threshold for significance of the |Correlation Factor| is 0.1859 at 0 days and 0.1865 at -1 days for 116 observations (Minitab LLC 2022). All other correlations were not significant.

Table 2.2. dLNdt-1 and dProductivitydt-1 Cross-Correlations

Lag (days)	dNEP dt^{-1}	dGPP dt^{-1}	dR dt^{-1}
-1	-0.342	-0.209	-
0	0.225	-	-0.202

A lag of -1 corresponds to the productivity one day after mixing. The significance threshold of |Correlation Factor| is >= 0.1859 at lag = 0 and 0.1865 at lag = -1. Insignificant correlations were omitted.

An additional correlation analysis was conducted between the daily averages of mixed layer depth, epilimnion temperature, radiation, and productivity, shown in Table 2.3. Spearman correlations were chosen as the analytical method as several relations appeared nonlinear but monotonic. All significant *P* values were < 0.017. Respiration and GPP were positively correlated with radiation and temperature, but negatively correlated with mixed layer depth. Net Ecosystem Production was positively correlated with mixing depth but negatively correlated with epilimnion temperature.

Table 2.3. Light, Mixing Depth, and Epilimnion Temperature Spearman Correlations

	Spearman Rho		
	Radiation	Mixed Layer Depth	Epi Temp
Mixed Layer Depth	-0.465	-	-
Epi Temp	0.539	-0.675	
R	0.225	-0.343	0.546
GPP	0.355	-0.254	0.497
NEP	-	0.241	-0.253

Correlations that were not significant to $p < 0.05$ were omitted. R was considered to be positive for this analysis.

Measured DOC values are shown in Table 2.4. Only four profiles were collected between May and October. At all depths, DOC exceeded 5 mg L^{-1} which is the threshold suggesting net heterotrophy by Prairie et al. (2002). There was no DOC data for October when the lake became net autotrophic.

Table 2.4. Measured 2019 DOC Concentrations (mg/L)

Date	Depth (m)		
	0	2	4
5/23	8.8	7.5	6.6
6/7	8.6	6.4	9.4
6/19	5.8	8	7.3
7/2	9.8	9.3	10.3

DOC concentrations at 0, 2 and 4-m depths. The values > 5 mg L^{-1} at 0-m depth suggest net heterotrophy according to Prairie et al (2002).

2.4 Discussion

Despite the hypereutrophic status of Goose Lake, the system exhibits net heterotrophy for most of the study period, as seen in Figure 2.3 and Table 2.1. This is likely due to the high DOC concentrations that are present, with observed surface concentrations ranging from 5.8 to 9.8 mg/L. A study of 33 Quebec lakes showed that lakes exhibit net heterotrophy when epilimnetic DOC concentrations are above 5 mg L^{-1} (Prarie and Bird 2002). The Goose Lake watershed is 11% wetlands, which may be a source of this DOC (Purdue University 2021).

October was the only month with a positive average NEP, marking a switch from net heterotrophy to net autotrophy. While GPP (rho = 0.355) is more strongly correlated with radiation than R (0.225), it is less sensitive to epilimnion temperature. The stronger correlation of temperature for R (0.546) than GPP (0.497) is consistent with other literature (Yvon-Durocher et al. 2010). NEP was negatively correlated with epilimnion temperature (-0.253) and not significantly correlated with light. This NEP correlation suggests that water temperature is a significant regulator of the ratio between GPP and R. Therefore, the cooler water temperatures in October may explain the switch to net autotrophy. Due to the lack of samples, it is unknown if DOC concentrations affected this switch.

Mixing depth is strongly negatively correlated with water temperature (rho = -0.675). Correlations between mixing depth and productivity may be spurious due to seasonality. The well-mixed, high-mixing depth period in the fall experiences lower light and water temperature, so decreases in productivity may be attributed to those factors. The

converse is true during warmer months, where stratified periods of high productivity experience high temperatures and incident radiation.

In support of our hypothesis, the cross-correlations showed that NEP and GPP increased one day after mixing. Mechanistically, this is likely due to nutrient-rich hypolimnetic waters mixing into the photic zone and causing an increase in photosynthesis. While there were no significant correlations two days after mixing, GPP and NEP may remain elevated. The correlation only measured the change in productivity from the previous day, so productivity would need to increase further on subsequent days after mixing for a signal to be visible. A multivariate analysis would be required to disentangle the effect of mixing from other processes which is beyond the scope of this analysis.

The decrease in NEP and increase in R on the day of mixing are likely due to an artifact of the diel oxygen technique. The DO sensor cannot measure below the mixed layer, so the analysis excludes respiration in the hypolimnion. When the lake mixes, this potentially hypoxic water enters the mixed layer, and the decrease in DO is calculated as respiration occurring on that day. Because increases in R directly reduce NEP, the calculated correlations agree with the expected signal.

These findings of increased GPP and NEP in response to mixings somewhat match those of Wilhelm and Adrian (2008), who showed an increase in algal biomass after mixing events. Their study found that maximum algal biomass was present three weeks after mixing. Their stratification periods in Lake Müggelsee were much longer than in this study, ranging from 1 week to 2 months. In contrast, Goose Lake stratified on the order of days, so there is the potential for increased drawdowns of DO in the hypolimnion and internal

loading in their system. Additionally, their study examined the longer-term increases in productivity as increased biomass, whereas this study can only observe initial changes in productivity through the cross-correlations. While suggesting similar results, both studies examine different pieces of the same puzzle.

Several limitations of the diel oxygen technique may impact the analysis. First, a core assumption is that respiration is constant between daylight and nighttime periods (Staehr et al. 2010). This results in lower calculated values of R and GPP but no change in NEP, as the changes to R and GPP are equal and opposite. Second, mixing processes (included in the A in Eq. 1) can cause noise in the productivity calculations. This was observed in the negative R values on October 15th and 16th. Staehr et al. (2010) recommend including negative values as a normal distribution should result in correct mean values on a monthly to seasonal scale. Because we were analyzing productivity on a daily time scale, we omitted those dates from the analysis. However, the presence of negative productivity values suggests that mixing processes are introducing error into the diel productivity calculations. This is likely due to the changing mixed layer depth affecting the oxygen mass balance, as was seen as the increased respiration on the day that mixing occurred. A depth integrated mass balance approach, such as that used in a more recent paper by Staehr et al. (2012) would have likely been more appropriate for a polymictic system. However, the project timeline did not allow for repeating the analysis. Finally, the diel oxygen technique assumes that the single sonde profile is representative of the entire horizontal lake area, likely introducing some error (Staehr et al. 2010).

Additional limitations of the study include low temporal resolution of nutrient sampling and using only a single year of data for a single lake. The temporal resolution of our nutrient sampling was low, and DOC was not analyzed later in the season. This omits the critical period where the lake becomes net heterotrophic in October. While our hypothesis proposes that increasing epilimnetic nutrient concentrations after mixing causes productivity increases, we have no direct measures of nutrient concentrations before or after mixing events. Finally, using a single year of data on a single lake complicates generalizing the results to other systems, and it is unknown if 2019 was a representative year biologically for the site.

2.5 Conclusions

Metabolism in Goose Lake was modeled via the diel oxygen technique for the 2019 field season. The change in the daily productivity values were cross correlated with Lake Number to examine delayed signals between mixing and productivity. It was found that GPP and NEP were negatively correlated with Lake Number one day after mixing. This suggests that productivity increases in polymictic lakes in response to mixing. This agrees with the findings of Wilhelm and Adrian (2008). Because mixing frequency impacts productivity, the subsequent chapter examines the impact on climate change on mixing frequency in Goose Lake.

3 Effects of Climate Change on Hydrodynamics in a Shallow, Hypereutrophic, Polymictic Lake

3.1 Background

Climate change is altering ecosystems globally with effects ranging from ocean acidification to changing precipitation patterns. A significant concern in lakes is that elevated air temperatures and shifting wind patterns may alter mixing frequencies and change the timing and duration of stratified summer periods (Kirillin 2010; Woolway and Merchant 2019). However, there is some uncertainty about the climatic response of shallow, polymictic lakes because increased wind forcing may offset stronger stratification due to warming, but reduced forcing would have the opposite effect (Woolway et al. 2017; Woolway and Merchant 2019). Understanding how lakes will respond to climate change is vital to informing management decisions, and lake hydrodynamics are foundational to other ecosystem processes.

Lakes stratify due to the formation of density gradients in the water column (Woolway and Merchant 2019). These gradients can be thermal, as in the case of warming surface waters, or chemical, as in saline lakes (Boehrer and Schultze 2008). Lakes mix when external forces overcome the density gradient; the external forces are generally wind and/or an increased density of surface waters. Increasing density is not limited to cooling, as fresh water is most dense at 4°C. A notable effect of this property in temperate regions is the occurrence of inverse stratification in winter, where water near the bottom is the warmest, and temperatures decrease as they approach the surface ice layer (Woolway et al. 2020). As a significant mass-transport process, lake mixing regulates other processes within lakes.

Two processes regulated by mixing are dissolved oxygen (DO) and nutrient transport (Woolway and Merchant 2019). Because only the water surface can exchange oxygen with the atmosphere, physical mixing is the main process that provides oxygen to deeper waters. Overturn also mixes nutrients from deeper waters into the photic zone, where they can be utilized by algae. During stratified periods, biological activity within sediments can deplete DO concentrations in the hypolimnion, releasing iron-bound phosphorus from sediments due to changing redox conditions (Sondergaard et al. 2001). This can stimulate internal loading of phosphorus and exacerbate eutrophication. Both DO and nutrient transport are expected to be impacted by altered mixing patterns due to climate change (O'Reilly et al. 2003; Adrian et al. 2009).

Climate change directly impacts the timing and frequency of lake mixing. In temperate regions, one direct result of increased air temperatures is the reduction of winter ice cover (Fang and Stefan 1998). When ice onset is delayed or ice extent reduced, the exposed darker water absorbs more radiation, warming the lake. However, warming can be counteracted by evaporative cooling and heat transfer with the atmosphere (Zhong et al. 2016). In the spring, warmer temperatures result in earlier ice-off, accelerating the onset of summer stratification. During the summer, warmer air temperatures heat surface waters, which strengthens stratification by increasing the vertical temperature gradient within the water column. Warmer fall temperatures cause this gradient to persist until cooling surface waters destabilize the water column and allow for mixing. If warming occurs to the point that ice does not form in the winter, it can cause a temperate dimictic lake to switch to a warm monomictic regime (Woolway and Merchant 2019; Woolway et al. 2020).

In addition to direct temperature forcing, trends in observed reductions of wind speeds in the northern hemisphere, known as atmospheric stilling, also have the potential to reduce mixing frequency and intensity (Woolway et al. 2017, 2019). However, increases in wind speeds are observed in some areas (Desai et al. 2009). Decreases in transparency can also strengthen stratification and can result from increased phytoplankton biomass, increased DOM, resuspended sediment, or erosion (Heiskanen et al. 2015; Pilla et al. 2018). However, the increased surface warming due to transparency decreases is most pronounced in clear lakes. The net effect of climate change in many lakes is elevated surface water temperatures and increased stratification, which can alter lake ecosystems.

Increased water temperatures and stratification induce many other changes in lake ecosystems. Higher water temperatures accelerate metabolic activity. However, respiration is more temperature dependent than photosynthesis, which will accelerate DO drawdowns (Cortés et al. 2021). Longer periods of stratification will decrease DO transport to the hypolimnion, which will increase stress on cold water fish and exacerbate internal loading of phosphorus (Sondergaard et al. 2001; Ficke et al. 2007). Additionally, elevated temperatures can directly stress fish and accelerate bioaccumulation of contaminants (Ficke et al. 2007). Cyanobacteria can cause nuisance blooms and thrive in warmer, stratified systems (Yankova et al. 2017; Bartosiewicz et al. 2019). Some species produce toxins that can harm aquatic life and human health. Cyanobacteria can manipulate their buoyancy, allowing them to obtain carbon dioxide directly from the atmosphere or phosphorus from lower waters (Bartosiewicz et al. 2019). Species that can fix nitrogen further outcompete other algae in high phosphorus environments. These adaptations allow them to outcompete other phytoplankton, impacting the food web. Finally, increased

stratification can decrease overall productivity due to reduced nutrient transport (O'Reilly et al. 2003).

Polymictic lakes are lakes that mix multiple times per year. They can be classified as continuous, where the lake is continuously mixed, or discontinuous, where the lake experiences periodic stratification throughout the year (Woolway et al. 2020). They are further divided into warm and cold based on the presence of winter ice cover. Polymictic lakes tend to be shallow, which causes increased sensitivity to wind forcing on mixing due to the lower mass of water (Woolway et al. 2017; Woolway and Merchant 2019). A modeling study by Woolway and Merchant (2019) forecasting changes in global mixing frequency due to climate change found that certain shallow lakes increased in mixing frequency despite the general trend of decreased mixing. A separate study by Kirillin (2010) found that water clarity was a key parameter determining the response of polymictic lakes to climate change. Darker waters absorb more light energy near the surface, strengthening the vertical thermal gradient. They modeled shifts in the currently polymictic Lake Müggelsee to a dimictic regime by midcentury and a warm monomictic regime by the end of the century. Additionally, they predicted that other temperate polymictic lakes would exhibit the same regime shift. However, polymictic lakes have variable responses to climate change, so further case studies are needed to illuminate lake-specific effects.

The objectives of this study are to model potential changes to mixing frequency and stratification duration in a temperate, shallow, hypereutrophic, polymictic lake between 2019 and early 2080's resulting from climate change. Additional objectives include

determining the model sensitivity to wind speed and water clarity because other studies have noted those as key parameters.

3.2 Methods

3.2.1 Study Site

Goose Lake is a small, shallow, polymictic lake located in Marquette Co., MI, shown in Figure 2.1. The lake is impaired for phosphorus as defined by the Clean Water Act Section 303(d) and is hypereutrophic due to historical discharges of untreated wastewater until 1953 (White Water Associates 2003; Holden 2011). Internal loading of phosphorus is still of concern today as a result of this discharge. The lake has a functional surface area of 1.69 km^2 with an average depth of 3.46 m and a maximum depth of 4.57 m. This surface area omits the southwestern basin on the far side of a railroad bridge, shown in Figure 2.1, which was not considered to be connected to the rest of the lake. Partridge Creek is the primary hydrologic input into the system, and the single outflow is aptly named Goose Lake Outlet. Two small, unnamed streams were not considered to be significant hydrologic inputs.

3.2.2 Field Methods and Data Acquisition

Continuous water profiles and weather data were collected through a five-month buoy deployment during the 2019 field season between 6/7 and 10/17. The buoy was deployed at the deepest point of Goose Lake and was equipped with an AIRMAR Weather Station 200WX at 1- m height. That sensor array monitored wind speed, air temperature, and pressure, and a LICOR pyranometer measured shortwave radiation. A thermistor chain suspended through the depth range of 0.5-4.5 m included NexSens thermistors at 0.5-m intervals and HOBO Dissolved Oxygen Loggers at 2 and 4-m depth. Finally, a YSI EXO2 sonde at 1-m depth was directly attached to the buoy. The sampling frequency for all instruments was 10 min.

Additional data about the site was obtained via stream gauging and third-party sources. A HOBO Water Level Logger was deployed at the mouth of Partridge Creek from 5/23 to 10/24 in order to calculate the daily streamflow. The streamflow was measured on four dates; 6/7, 6/19, 7/2, and 7/25 with a USGS Pygmy Current Meter. However, only the latter three measurements were used in the rating curve because 6/7 was an outlier. The Goose Lake Outlet was not gauged or monitored. Daily precipitation time series were accessed from the NOAA Marquette WFO station and relative humidity time series from the Chatham 1 SE station in Alger Co., MI (2022; Purdue University and NOAA 2023). These stations are located 7 km north and 48 km southeast of the lake, respectively, but were the closest locations with available data. Lake bathymetry was derived from a Navionics SonarChart™ map (2021).

A continuous, smoothed weather dataset was required for the model input. Twenty-four-hour gaps in buoy observations, which began at 16:00 on the last day of each month, were present. These periods were filled by substituting in the observations from the previous days. Wind data was smoothed by removing any 10 min periods recording windspeeds > 20 m/s and filling the gaps via linear interpolation. These cleaned datasets were averaged to a one-hour timestep and used to construct a one-dimensional hydrodynamic model of the system.

3.2.3 Model Description

The one-dimensional, vertically integrated General Lake Model (GLM) was selected to simulate lake hydrodynamics. The General Lake Model is the successor to the Dynamics Reservoir Simulation Model (DYRESM) and has been applied in settings

ranging from wetlands to large lakes (Hipsey et al. 2019). A brief overview of the model requirements will be included here. For a full description of calculation methods, refer to Hipsey et al. (2019). This analysis used GLM version 3.1.0a4.

Data required to drive the model includes lake morphometry, an initial temperature profile, inflow water temperature, precipitation, and high-resolution air temperature, wind speed, shortwave radiation, and relative humidity inputs. In place of the outflow module, the crest height of the lake was set to the maximum depth of 4.57 meters so the lake would "spill over" when full as a pseudo-outflow. This approach maintains a consistent water level and may not accurately reflect levels in dry periods. Due to the lack of longwave radiation data, the Bird Clear Sky Method was used with default parameters to estimate longwave radiation and cloud cover from measured shortwave radiation. An annotated configuration file detailing calculation method selection is provided in the appendix.

3.2.4 Model Calibration

Simulated annealing was selected as the optimization method for the GLM model to calibrate the model to observed temperature profiles and stability indices (Kirkpatrick et al. 1983). This autocalibration approach uses an evolutionary algorithm to minimize a multivariate function while avoiding local minima. This optimization was applied using the GenSA package in R (Xiang et al. 2013; R Core Team 2022). All code for the autocalibration is included in the appendix. The following cost function was calculated as the sum of the weighted Normalized Root Mean Squared Errors (NRMSE) between observed and modeled water temperature and Lake Number (LN).

$$Model\ NRMSE = x * (Temperature\ NRMSE) + y * (Lake\ Number\ NRMSE)$$

[3.1]

Where x and y are decimal weights that always sum to 1.

Lake Number, a measure of water column stability, was included in the cost function to improve the vertical distribution of heat throughout the water column (Robertson and Imberger 1994). Lake Number is an index of mixing potential calculated using Schmidt Stability and wind conditions, explained further in Chapter 1. Lake Number was calculated using the LakeAnalyzer package in R (Read et al. 2011). Their approach uses the top and bottom metalimnion depths in the calculation. In our application, the minimum metalimnion temperature gradient was set to zero to prevent the function from returning null values during mixed periods. The resulting LN values approached zero which would be expected under mixed conditions. Any negative LN values for these periods were assumed to be zero since the lake would be well mixed.

During the calibration, the model was run continuously at a one-hour timestep from 6/8/19 to 10/17/19. Nine GLM parameters were selected for calibration and are listed in Table 3.2, along with their allowed ranges and default values. The bounds were set narrowly so the combined outputs would remain at realistic values. For example, the shortwave factor is a scalar, so the bounds were set to the narrow range of 70% to 130%. Parameters for internal mixing were set to default values, and stream parameters from the Kinneret example file were used (Bruce et al. 2018). Each calibration run was set to 5000 iterations, though some runs exceeded this target. Weights were applied to the NRMSE

cost functions, ranging from 50% temperature and 50% LN to 100% temperature and 0% LN in 10% increments. However, the 0% LN sets were not considered in the final analysis. Four runs were conducted for each set of weights. Model validation was not possible as we had only one season of data. Therefore, we selected the best calibration run based on the lowest Root Mean Squared Error (RMSE) for temperature.

3.2.5 Model Application

In order to run models of future scenarios, high-resolution weather data was required, as noted above. Six future forecasts from the World Climate Research Programme's Coupled Model Intercomparison Project 5 (CMIP5) database were selected for the RCP4.5 and 8.5 middle to high emissions scenarios. The 2080 outputs for the GFDL-CM3 and GFDL-ESM2M models and 2081 outputs for MIROC5 were used (Taylor et al. 2012). These models were determined to perform well in the Great Lakes Region by Byun and Hamlet (2018) based on historical accuracy. In the case of MIROC5 which had multiple ensemble outputs, only the r1i1p1 was used in this analysis. These climate model outputs were available at a 3-hour temporal resolution and 2-degree latitude and 2.5-degree longitude grid size. The climate model grid centroid was 0.455 degrees north and 0.333 degrees west of the study site.

Several derived parameters and assumptions were required to compensate for missing variables in the climate projections. Relative humidity time series were not directly available and had to be estimated from specific humidity, temperature, and air pressure using the Bolton method (Bolton 1980). The future inflow for Partridge Creek was assumed to match the observed 2019 distribution. That observed daily flow was multiplied by the

ratio of total precipitation between the future and 2019 study periods. While the resulting hydrograph does not correspond to future precipitation events, scaled flow rates were examined in the sensitivity analysis. The initial 2019 profile was used with a 1-week model spin-up period because there was no way to estimate an initial water temperature profile. This period was deemed adequate due to the shallow lake depth, which should allow temperatures to reach equilibrium quickly. The inflow temperature was forecasted using a linear regression between air and water temperature on the 2019 data. The 3-hour climate model datasets were linearly interpolated to a 1-hour timestep to be compatible with GLM.

Finally, the future models were run from 6/1 to 10/17 at a 1-hour timestep. Key model outputs included 1-m and 4-m water temperatures, the number of mixings events, the longest continuous period of stratification, and the percentage of the study period that was stratified. Mixing events were defined as consecutive periods where the LN transitioned from >1 to <1. Lake Number was calculated using 3-hour averaged data to reduce noise. Mixing events and mixed periods were identified using the Run Length Encoding function in R (R Core Team 2022). This function calculates how many consecutive entries in a series match a given condition, in this case if LN >1. Sensitivity analyses were performed for wind speed, transparency (K_W), and Partridge Creek inflow. The former two are parameters of interest based on the studies by Kirillin (2010), Woolway et al. (2017) and Woolway and Merchant (2019). The Partridge Creek inflow curve assumption is a potential source of error, so it was also analyzed. The 2019 calibration and GFDL-CM3 scenarios were run with ± 10, 25, and 50% variation in calibrated values.

3.2.6 Climactic Inputs

While this analysis is limited due to only a single year of field data, the 2019 study period aligns with recent climatic trends. The June – October 2019 temperature observations at the buoy were 0.29 °C warmer than the 2006-2020 reference average for the Marquette WFO station, shown in Table 3.1 (NOAA 2023). Precipitation was elevated by 1.67 cm in 2019 compared to the reference period. Averages for windspeed and shortwave radiation were not available for this station. These climactic averages show that 2019 is a reasonable year on which to base future comparisons.

Table 3.1. Study Period Climate Averages

	2006-2020 Average	2019 Observed
Temp (C)	15.22	14.93
Precip (cm)	40.62	42.29

3.3 Results

The best set of calibrated GLM parameters, along with their bounds and default values, are listed in Table 3.2. The weights for the run were 80% temperature and 20% LN. The summed NRMSE was 0.378, the temperature RMSE was 1.424 °C, and the LN RMSE was 0.943. This calibration set was selected because it had the lowest temperature RMSE out of all the runs with an LN weight > 0. The resulting wind, shortwave, air temperature, and relative humidity factors were reduced, while longwave factor was increased. Coefficients for sensible and latent heat, C_E and C_H, were increased while wind drag, C_D, was decreased. Light extinction, K_W, was high at 3.287 m^{-1}.

The corresponding 2019 GLM output is shown in Figure 3.1. The lake was well mixed for the majority of the season, experiencing stratification only 4.4% of the study period. The average temperature at 1 m was 19.93 °C, 4 m was 19.66 °C, and the ΔT was 0.27 °C. The lake experienced 19 mixing events, and the longest consecutive period of stratification was 15 hours. These mixing behaviors and calibration parameters were used as a reference for the future model outputs and sensitivity analyses.

Table 3.2. GLM Calibrated Parameters

Parameter	Value	Default	Min	Max
Wind Factor	0.7115	1.0	0.7	1.3
Shortwave Factor	1.0246	1.0	0.7	1.3
Longwave Factor	0.8370	1.0	0.7	1.3
Air Temperature Factor	0.7872	1.0	0.7	1.3
Relative Humidity Factor	0.9565	1.0	0.9	1.1
Latent Heat C_E	0.0015	0.0013	0.0011	0.0015
Sensible Heat C_H	0.0015	0.0013	0.0011	0.0016
Momentum Transfer. C_D	0.0011	0.0013	0.0011	0.0015
Light Extinction K_W (m^{-1})	3.2869	-	0.5	5

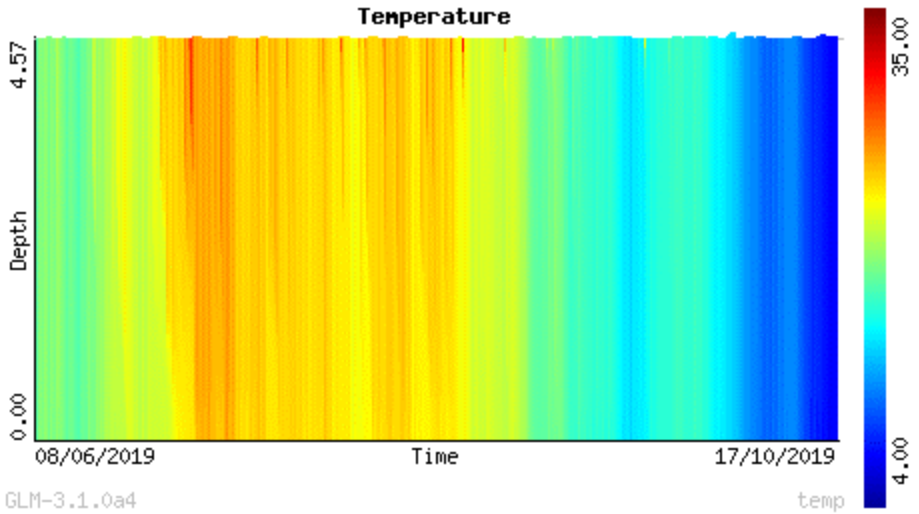

Figure 3.1. 2019 Modeled Temperature Profile

Future climactic drivers, shown in Table 3.3, varied significantly relative to 2019. All future models had lower average wind speeds during the study period, which match the currently observed atmospheric stilling phenomenon (Woolway et al. 2019). Precipitation was variable, with only the GFDL-CM3 8.5 and MIROC5 8.5 models experiencing elevated levels. The average air temperature increases for the RCP 4.5 and 8.5 scenarios were 6.74 °C and 8.46 °C, respectively. Shortwave radiation was 7.4 to 14.4% higher in all models.

Table 3.3. Change in Climate Drivers Relative to 2019

Model	Precipitation	Shortwave Radiation	Δ Air Temperature (C)	Wind Speed
GFDL-CM3 4_5	91.0%	110.8%	6.94	74.0%
GFDL-CM3 8_5	117.7%	112.1%	9.49	67.1%
GFDL-ESM2M 4_5	90.8%	107.4%	7.06	73.2%
GFDL-ESM2M 8_5	84.8%	113.7%	7.85	75.5%
MIROC5 4_5	70.8%	112.2%	6.23	57.7%
MIROC5 8_5	114.2%	114.4%	8.04	53.4%

In all future scenarios, water temperatures, mixing frequencies, and stratification extent increased relative to 2019. Model outputs and analyses are shown in Figure 3.2 and Table 3.4. Average 1 m temperature increases were 5.71 °C for the RCP 4.5 scenarios and 7.06 °C for the RCP 8.5 scenarios. These water temperature increases were 84.7% and 84.1% of air temperature increases for the two scenarios, respectively. Average ΔT between 1 and 4 m increased by 1.18 °C and 1.64 °C for the 4.5 and 8.5 scenarios. While the longest consecutive period of stratification was 15 hours in 2019, future models ranged from 69 to 258 hours. Finally, the percentage of the study period that was stratified increased from 4.4% in 2019 to between 16.7 and 42.8% in the future scenarios.

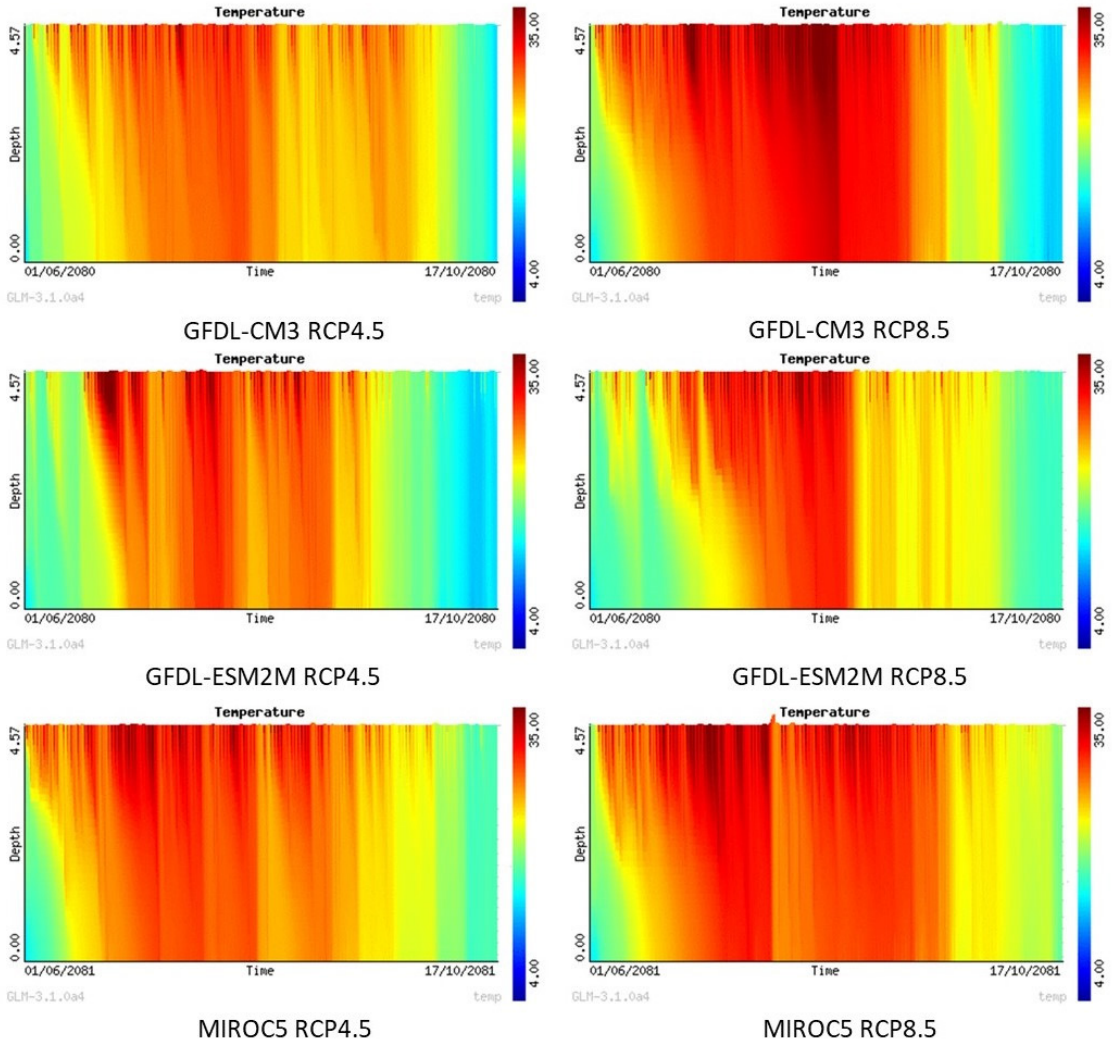

Figure 3.2. Future Model Temperature Profile.

Both GFDL scenarios are for 2080 while MIROC5 is 2081. These profiles include the 1-week spin-up period.

Table 3.4. Future Scenario Analyses

Scenario	# of Mixing Events	Longest Strat (Hours)	% Stratified	1m Avg Temp (C)	4m Avg Temp (C)	Δ T (C)
2019	19	15	4.4%	19.93	19.66	0.27
GFDL-CM3 4.5	27	69	16.7%	25.57	24.41	1.16
GFDL-CM3 8.5	35	150	31.8%	27.75	25.95	1.80
GFDL-ESM2M 4.5	21	177	16.1%	24.65	23.24	1.41
GFDL-ESM2M 8.5	26	90	24.2%	25.17	23.18	1.99
MIROC5 4.5	63	258	39.1%	26.71	24.93	1.79
MIROC5 8.5	62	195	42.8%	28.22	26.29	1.93

Sensitivity analyses for wind speed, K_W, and Partridge inflow for the 2019 and GFDL-CM3 scenarios were conducted to measure their impact on stratification extent throughout the study period. Plots of these outputs are shown in Figure 3.3. The GLM model was sensitive to decreases in wind speed, which agrees with the findings of Woolway et al. (2017) in polymictic lakes. This trend is notable because all future scenarios had decreased wind speeds relative to 2019. Scaling K_W did not produce a high variation in stratification, contrary to the findings of Kirillin (2010). Interestingly, there is a slight negative trend between K_W and stratification, which is the opposite of typical assumptions (Pilla et al. 2018). Scaling the Partridge Creek Inflow did not significantly influence stratification duration.

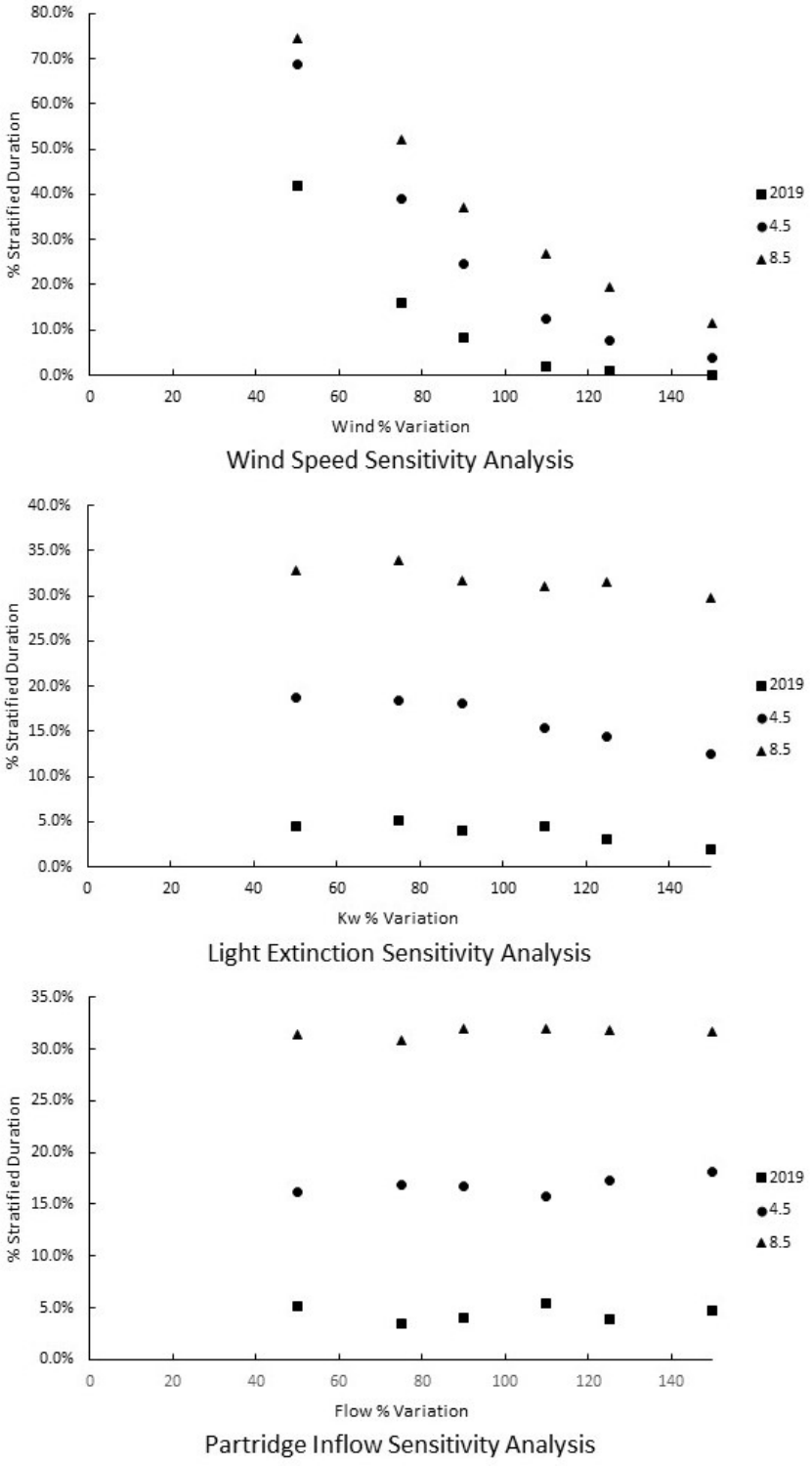

Figure 3.3. Stratification Extent Sensitivity Analysis

3.4 Discussion

The 2019 model simulation yielded a well-mixed lake for most of the study period but had few mixing events. While these outcomes may seem contradictory, they can be attributed to how mixing was defined in this analysis. A mixing event was quantified as a shift from stratified to mixed conditions. Because Goose Lake was well mixed for 95.6% of the study period, there were few opportunities for recovery from stratification. When considering the results of the future models, the number of mixing events tended to increase with stratification extent. However, there is likely a stratification threshold where mixing events would rapidly decrease, which was not reached in this study.

The model parameters have competing effects on lake hydrodynamics. These parameters are listed in Table 3.2. The input variable scalars of wind, longwave, air temperature, and relative humidity factors were reduced, while the shortwave factor was increased by 2.5%. The reduction in wind factor to 71.2% limits wind availability for mixing and evaporation (Hipsey et al. 2019). This considerable reduction of the observed time series is likely a result of wind sheltering being disabled in the model configuration. Sheltering lowers wind speeds above small lakes, especially in nearshore areas, and the buoy was placed in the middle of the lake where wind speeds would be highest (Holgerson et al. 2022). Longwave radiation was not directly measured and was estimated by GLM using shortwave radiation and the Bird Clear Sky Model (Hipsey et al. 2019). The 83.7% would decrease the cloud cover calculated by the model, cooling the lake. The lower relative humidity scalar of 95.7% would increase evaporation and, therefore, evaporative cooling (Hipsey et al. 2019). The slight reduction may result from the off-site relative

humidity data that was used. Finally, the 102.5% shortwave radiation scalar would have a direct warming effect on the lake.

Parameters used to calculate latent and sensible heat, C_E and C_H, were both elevated from the default values. An elevated C_E results in greater evaporative cooling, while increased C_H would have a net cooling effect because the average air temperature for the study period was lower than the 1-m water temperature. The bulk transfer coefficient for momentum, C_D, was below the default value. This change would reduce mixing by limiting the amount of energy that wind imparts on the lake and may also be a result of disabled wind sheltering. While reductions in wind factor would affect both mixing and evaporation, C_D would only impact mixing (Hipsey et al. 2019). Light extinction, K_W, was high at 3.287 m^{-1}, which would increase surface warming and stratification through light attenuation in near-surface waters. Despite competing forces in the calibration parameters, the future models resulted in elevated water temperatures and stratification.

The model was extremely sensitive to wind speed decreases for both 2019 and 2080 scenarios, which is in agreement with a modeling study by Woolway et al. (2017) on polymictic lake Võrtsjärv. Because all future scenarios had lower wind speeds than in 2019, much of the increase in stratification can likely be attributed to this trend. For example, both MIROC5 scenarios had the highest stratification extent out of all models at 39.1% and 42.8% for the RCP 4.5 and 8.5 scenarios, respectively, but had the lowest average wind speeds, only 57.7% and 53.4% of 2019. It is notable that Goose Lake does not shift mixing regimes despite reduced wind speed because the predictions by Kirillin (2010) assumed unchanged future windspeeds above Müggelsee.

Even under significant warming, it does not appear that Goose Lake will shift mixing regimes by 2080. The longest continuous period of stratification between all the models was 10.75 days for the MIROC5 RCP 4.5, and the model with the lowest mixing frequency was the GFDL-ESM2M 4.5 with 21 mixing events. These fall far short of the predictions by Kirillin (2010) of shifts to dimictic regimes, defined by 120 consecutive days of summer stratification by midcentury in temperate, polymictic lakes. However, the increase in bottom temperatures in all models is consistent with their 2100 prediction, despite the lack of a monomictic regime.

There are several reasons why the projected mixing behaviors of the lakes may differ. The first may be the low depth of Goose Lake (3.6 m avg. 4.6 m max) relative to Müggelsee (4.9 m avg. 8.0 m max) (Kirillin 2010). Less wind energy is required to mix a shallow lake completely than in a deeper lake. Second, differences in transparency may play a role. While Kirillin found that changing transparency greatly affected lake mixing behavior, the K_W sensitivity analysis for Goose Lake did not. The K_W in Goose Lake was 3.29 m^{-1}, more than double that of Müggelsee at 1.2 m^{-1}. The already high K_W may be to blame for the low sensitivity. A study by Pilla et al. (2018) that compared historical warming and stratification dynamics in two small lakes found that the initially more turbid lake was less impacted by further decreases in transparency than a similar clear lake. A separate study by Heiskanen et al. (2015) found high model sensitivity for $K_W < 0.5$ m^{-1} in 1-D LAKE and FLake models.

The calibrated K_W was high, at 3.29 m^{-1}. However, it is not unrealistic for this system because the lake is hypereutrophic and impaired for phosphorus, resulting in high

algal biomass. While no Secchi depths were taken during fieldwork for this study, depths of 1.2 m and 0.6 m were measured in August of 2003 and 2006 during the Goose Lake Nutrient Study and TMDL fieldwork (White Water Associates 2003; Holden 2011). For the latter depth, the Poole and Atkins relation between Secchi depth and K_W yields a K_W of 2.94 m^{-1}, which approaches the calibrated GLM parameter (Society 2008).

The high K_W poses some challenges to the experimental design. According to the Beer-Lambert law, the resulting depth of the euphotic zone for the calibrated K_W would be 1.40 m. This analysis only considered temperatures starting at 1-m depth in the calibration and subsequent calculations because it matched to match our observed data. Therefore, if the top of the metalimnion is less than one meter deep due to intense light attenuation in the euphotic zone, as may be the case in the sensitivity analysis with the maximum Kw of 4.93 m^{-1}, that period would be calculated as non-stratified. This phenomenon could explain the slight trend of decreasing stratification with increasing K_W values in the sensitivity analysis.

Despite retaining a polymictic regime, increased stratification and warmer water temperatures will likely exacerbate existing water quality problems in Goose Lake. While the stratified periods are still relatively short compared to dimictic lakes, these events can still result in hypoxia. In eutrophic, polymictic lakes Kasumigaura and Kitaura in Japan, a study by Fukushima et al. (2019) observed DO demand of 4.3 mg L^{-1} d^{-1} before stratification events that resulted in DO concentrations < 2 mg L^{-1}. Increased hypoxia will stimulate internal loading of phosphorus, which along with elevated temperatures, will increase favorability for buoyant cyanobacteria (Sondergaard et al. 2001; Bartosiewicz et

al. 2019). Algal blooms can further draw down DO as a positive feedback loop. Finally, fish kills have previously been observed in Goose Lake, and increased DO drawdowns and temperature stress may exacerbate this phenomenon (Ficke et al. 2007; Holden 2011).

One question not addressed in this study is the potential of a regime shift from discontinuous cold polymictic to discontinuous warm polymictic. Increased winter temperatures directly affect ice cover, with loss of ice cover being a hallmark of regime change. A year-round monitoring project on Goose Lake would allow continuous modeling throughout the winter to examine changes in ice dynamics and summer stratification onset. Finally, additional monitoring would provide a validation dataset for the model developed in this study. Additionally, while no regime shift was observed in this case study of a single shallow, polymictic lake, this analysis should be expanded to other systems to understand the trends in variable climactic response of this extremely common lake type.

3.5 Conclusions

The 1-D General Lake Model was applied to Goose Lake and calibrated to the 2019 field season. Six CMIP5 climate outputs for the early 2080's were input to the model to examine potential changes to mixing frequency. In all future scenarios, mixing frequency was found to increase along with water temperatures and stratification extent. However, the lake remained polymictic despite warming. The model was extremely sensitive to changes in wind speed but insensitive to K_w, likely due to already low water clarity (Pilla et al. 2018). Increased warming and stratification will likely exacerbate existing water quality issues in Goose Lake by stimulating DO drawdowns, increasing internal loading of phosphorus, and providing favorable conditions for cyanobacteria (Sondergaard et al. 2001; Adrian et al. 2009; Bartosiewicz et al. 2019). Additional research is required to determine the impact of climate change on winter ice cover and the timing of summer stratification.

4 References

Adrian, R., C. M. O'Reilly, H. Zagarese, and others. 2009. Lakes as sentinels of climate change. Limnol. Oceanogr. **54**: 2283–2297. doi:10.4319/lo.2009.54.6_part_2.2283

Bartosiewicz, M., A. Przytulska, B. N. Deshpande, D. Antoniades, A. Cortes, S. MacIntyre, M. F. Lehmann, and I. Laurion. 2019. Effects of climate change and episodic heat events on cyanobacteria in a eutrophic polymictic lake. Sci. Total Environ. **693**: 133414. doi:10.1016/j.scitotenv.2019.07.220

Boehrer, B., and M. Schultze. 2008. Stratification of lakes. Rev. Geophys. **46**: 1–27. doi:10.1029/2006RG000210

Bolton, D. 1980. The Computation of Equvalent Potential Temperature. Mon. Weather Rev. **108**: 1046–1053. doi:https://doi.org/10.1175/1520-0493(1980)108<1046:TCOEPT>2.0.CO;2

Bruce, L. C., M. A. Frassl, G. B. Arhonditsis, and others. 2018. A multi-lake comparative analysis of the General Lake Model (GLM): Stress-testing across a global observatory network. Environ. Model. Softw. **102**: 274–291. doi:10.1016/j.envsoft.2017.11.016

Butcher, J. B., D. Nover, T. E. Johnson, and C. M. Clark. 2015. Sensitivity of lake thermal and mixing dynamics to climate change. Clim. Change **129**: 295–305. doi:10.1007/s10584-015-1326-1

Byun, K., and A. F. Hamlet. 2018. Projected changes in future climate over the Midwest and Great Lakes region using downscaled CMIP5 ensembles. Int. J. Climatol. **38**: e531–e553. doi:10.1002/joc.5388

Cole, J. J., Y. T. Prairie, N. F. Caraco, and others. 2007. Plumbing the global carbon cycle: Integrating inland waters into the terrestrial carbon budget. Ecosystems **10**: 171–184. doi:10.1007/s10021-006-9013-8

Cortés, A., A. L. Forrest, S. Sadro, A. J. Stang, M. Swann, and N. T. Framsted. 2021. Prediction of Hypoxia in Eutrophic Polymictic Lakes. Water Resour. Res. **57**. doi:10.1029/2020WR028693

Desai, A. R., J. A. Austin, V. Bennington, and G. A. McKinley. 2009. Stronger winds over a large lake in response to weakening air-to-lake temperature gradient. Nat. Geosci. **2**: 855–858. doi:10.1038/ngeo693

Fang, X., and H. G. Stefan. 1998. Potential climate warming effects on ice covers of small lakes in the contiguous U.S. Cold Reg. Sci. Technol. **27**: 119–140. doi:10.1016/S0165-232X(97)00027-X

Ficke, A. D., C. A. Myrick, and L. J. Hansen. 2007. Potential impacts of global climate

change on freshwater fisheries. Rev. Fish Biol. Fish. **17**: 581–613. doi:10.1007/s11160-007-9059-5

Fukushima, T., T. Kitamura, S. Komuro, K. Nakagawa, Y. Nagahama, S. Matsumoto, and B. Matsushita. 2019. Characteristics of declining dissolved oxygen concentrations in Lakes Kasumigaura and Kitaura , two shallow polymictic eutrophic lakes in Japan. Lakes Reserv. **24**: 314–323. doi:10.1111/lre.12294

Harrell Jr., F. E. 2022. Hmisc: Harrell Miscellaneous.

Heiskanen, J. J., I. Mammarella, A. Ojala, and others. 2015. Effects of water clarity on lake stratification and lake-atmosphere heat exchange. J. Geophys. Res. Ocean. **120**: 1–17. doi:10.1002/2014JD022938

Hipsey, M. R., L. C. Bruce, C. Boon, and others. 2019. A General Lake Model (GLM 3 . 0) for linking with high-frequency sensor data from the Global Lake Ecological Observatory Network (GLEON). Geosci. Model Dev. **12**: 473–523. doi:10.5194/gmd-12-473-2019

Holden, S. 2011. Total Phosphorus Total Maximum Daily Load for Goose Lake Marquette County, Michigan.

Holgerson, M. A., D. C. Richardson, J. Roith, and others. 2022. Classifying Mixing Regimes in Ponds and Shallow Lakes. Water Resour. Res. **58**: 1–18. doi:10.1029/2022WR032522

Idso, S. B. 1973. On the Concept of Lake Stability. Limnol. Oceanogr. **18**: 681–683. doi:10.4319/lo.1973.18.4.0681

Kirillin, G. 2010. Modeling the impact of global warming on water temperature and seasonal mixing regimes in small temperate lakes. Boreal Environ. Res. **15**: 279–293.

Kirkpatrick, A. S., C. D. Gelatt, M. P. Vecchi, S. Science, N. Series, and N. May. 1983. Optimization by Simulated Annealing Published by : American Association for the Advancement of Science Stable URL : http://www.jstor.com/stable/1690046. Science (80-.). **220**: 671–680.

Laas, A., P. Nõges, T. Kõiv, and T. Nõges. 2012. High-frequency metabolism study in a large and shallow temperate lake reveals seasonal switching between net autotrophy and net heterotrophy. Hydrobiologia **694**: 57–74. doi:10.1007/s10750-012-1131-z

Lovett, G. M., J. J. Cole, and M. L. Pace. 2006. Is net ecosystem production equal to ecosystem carbon accumulation? Ecosystems **9**: 152–155. doi:10.1007/s10021-005-0036-3

Minitab LLC. 2022. Minitab Documentation.

NOAA. 2023. NOAA Climate Normals 2006-2020 Marquette WFO.

Nürnberg, G. K. 1998. Prediction of annual and seasonal phosphorus concentrations in stratified and polymictic lakes. Limnol. Oceanogr. **43**: 1544–1552. doi:10.4319/lo.1998.43.7.1544

O'Reilly, C. M., S. R. Alin, and P. Plisnier. 2003. Climate change decreases aquatic ecosystem productivity of Lake Tanganyika , Africa. Nature **424**: 766–768. doi:10.1038/nature01833

Pilla, R. M., C. E. Williamson, J. Zhang, R. L. Smyth, J. D. Lenters, J. A. Brentrup, L. B. Knoll, and T. J. Fisher. 2018. Browning-Related Decreases in Water Transparency Lead to Long-Term Increases in Surface Water Temperature and Thermal Stratification in Two Small Lakes. J. Geophys. Res. Biogeosciences **123**: 1651–1665. doi:10.1029/2017JG004321

Prarie, Y. T., and D. F. Bird. 2002. The summer metabolic balance in the epilimnion of southeastern Quebec lakes. Limnol. Ocean. **47**: 316–321.

Purdue University. 2021. L-THIA Great Lakes Watershed Management System.

Purdue University, and NOAA. 2023. Midwest Regional Climate Center Chatham 1 SE Alger MI.

R Core Team. 2022. R: A Language and Environment for Statistical Computing.

Read, J. S., D. P. Hamilton, I. D. Jones, K. Muraoka, L. A. Winslow, R. Kroiss, C. H. Wu, and E. Gaiser. 2011. Derivation of lake mixing and stratification indices from high-resolution lake buoy data. Environ. Model. Softw. **26**: 1325–1336. doi:10.1016/j.envsoft.2011.05.006

Robertson, D. M., and J. Imberger. 1994. Lake Number, a Quantitative Indicator of Mixing Used to Estimate Changes in Dissolved Oxygen. Int. Rev. der gesamten Hydrobiol. und Hydrogr. **79**: 159–176. doi:10.1002/iroh.19940790202

Rose, K. C., L. A. Winslow, J. S. Read, and G. J. A. Hansen. 2016. Climate-induced warming of lakes can be either amplified or suppressed by trends in water clarity. Limnol. Oceanogr. Lett. **1**: 44–53. doi:10.1002/lol2.10027

Schmid, M., and J. Read. 2022. Heat Budget of Lakes. Encycl. Inl. Waters 467–473. doi:10.1016/b978-0-12-819166-8.00011-6

Society, B. E. 2008. On the Universality of the Poole and Atkins Secchi Disk-Light Extinction Equation Author (s): Sherwood B . Idso and R . Gene Gilbert Published by : British Ecological Society Stable URL : http://www.jstor.org/stable/2402029. Society **11**: 399–401.

Sondergaard, M., P. J. Jensen, and E. Jeppesen. 2001. Retention and internal loading of phosphorus in shallow, eutrophic lakes. ScientificWorldJournal. **1**: 427–442. doi:10.1100/tsw.2001.72

Staehr, P. A., D. Bade, G. R. Koch, C. Williamson, P. Hanson, J. J. Cole, and T. Kratz. 2010. OCEANOGRAPHY : METHODS Lake metabolism and the diel oxygen technique : State of the. Limnol. Ocean. Methods **8**: 628–644. doi:10.4319/lom.2010.8.628

Staehr, P. A., L. S. Brighenti, M. Honti, J. Christensen, and K. C. Rose. 2016. Global patterns of light saturation and photoinhibition of lake primary production. Inl. Waters **6**: 593–607. doi:10.1080/IW-6.4.888

Staehr, P. A., J. P. A. Christensen, R. D. Batt, and J. S. Read. 2012. Ecosystem metabolism in a stratified lake. **57**: 1317–1330. doi:10.4319/lo.2012.57.5.1317

Staehr, P. A., and K. Sand-Jensen. 2007. Temporal dynamics and regulation of lake metabolism. Limnol. Oceanogr. **52**: 108–120. doi:10.4319/lo.2007.52.1.0108

Taylor, K. E., R. J. Stouffer, and G. A. Meehl. 2012. An overview of CMIP5 and the experiment design. Bull. Am. Meteorol. Soc. **93**: 485–498. doi:10.1175/BAMS-D-11-00094.1

Torremorell, A., M. E. Llames, G. L. PÉrez, R. Escaray, J. Bustingorry, and H. Zagarese. 2009. Annual patterns of phytoplankton density and primary production in a large, shallow lake: The central role of light. Freshw. Biol. **54**: 437–449. doi:10.1111/j.1365-2427.2008.02119.x

Tranvik, L. J., J. A. Downing, J. B. Cotner, and others. 2009. Lakes and reservoirs as regulators of carbon cycling and climate. Limnol. Ocean. **54**: 2298–2314. doi:10.4319/lo.2009.54.6_part_2.2298

Turan, G. S., and N. Karakaya. 2017. Determining lake metabolism using diel Oxygen technique: A case study of Lake Abant. Fresenius Environ. Bull. **26**: 7114–7121.

White Water Associates. 2003. Goose Lake Nutrient Study (Marquette County , Michigan).

Wilhelm, S., and R. Adrian. 2008. Impact of summer warming on the thermal characteristics of a polymictic lake and consequences for oxygen, nutrients and phytoplankton. Freshw. Biol. **53**: 226–237. doi:10.1111/j.1365-2427.2007.01887.x

Woolway, R. I., B. M. Kraemer, J. D. Lenters, C. J. Merchant, C. M. O'Reilly, and S. Sharma. 2020. Global lake responses to climate change. Nat. Rev. Earth Environ. **1**: 388–403. doi:10.1038/s43017-020-0067-5

Woolway, R. I., P. Meinson, P. Nõges, I. D. Jones, and A. Laas. 2017. Atmospheric

stilling leads to prolonged thermal stratification in a large shallow polymictic lake. Clim. Change **141**: 759–773. doi:10.1007/s10584-017-1909-0

Woolway, R. I., and C. J. Merchant. 2019. Worldwide alteration of lake mixing regimes in response to climate change. Nat. Geosci. **12**: 271–276. doi:10.1038/s41561-019-0322-x

Woolway, R. I., C. J. Merchant, J. Van Den Hoek, C. Azorin-Molina, P. Nõges, A. Laas, E. B. Mackay, and I. D. Jones. 2019. Northern Hemisphere Atmospheric Stilling Accelerates Lake Thermal Responses to a Warming World. Geophys. Res. Lett. **46**: 11983–11992. doi:10.1029/2019GL082752

Xiang, Y., S. Gubian, B. Suomela, and J. Hoeng. 2013. Generalized Simulated Annealing for Efficient Global Optimization: the {GenSA} Package for {R}.

Yankova, Y., S. Neuenschwander, O. Köster, and T. Posch. 2017. Abrupt stop of deep water turnover with lake warming: Drastic consequences for algal primary producers /631/158/2165 /704/106/286 article. Sci. Rep. **7**: 1–9. doi:10.1038/s41598-017-13159-9

Yvon-Durocher, G., J. I. Jones, M. Trimmer, G. Woodward, and J. M. Montoya. 2010. Warming alters the metabolic balance of ecosystems. Phil. Trans. R. Soc. **365**: 2117–2126. doi:10.1098/rstb.2010.0038

Zhong, Y., M. Notaro, S. J. Vavrus, and M. J. Foster. 2016. Recent accelerated warming of the Laurentian Great Lakes: Physical drivers. Limnol. Oceanogr. **61**: 1762–1786. doi:10.1002/lno.10331

2021. Goose Lake Batyhmetry. Navionics.

2022. NOWData -NOAA Online Weather Data. Natl. Weather Serv.

5 Appendix

5.1 Goose Lake

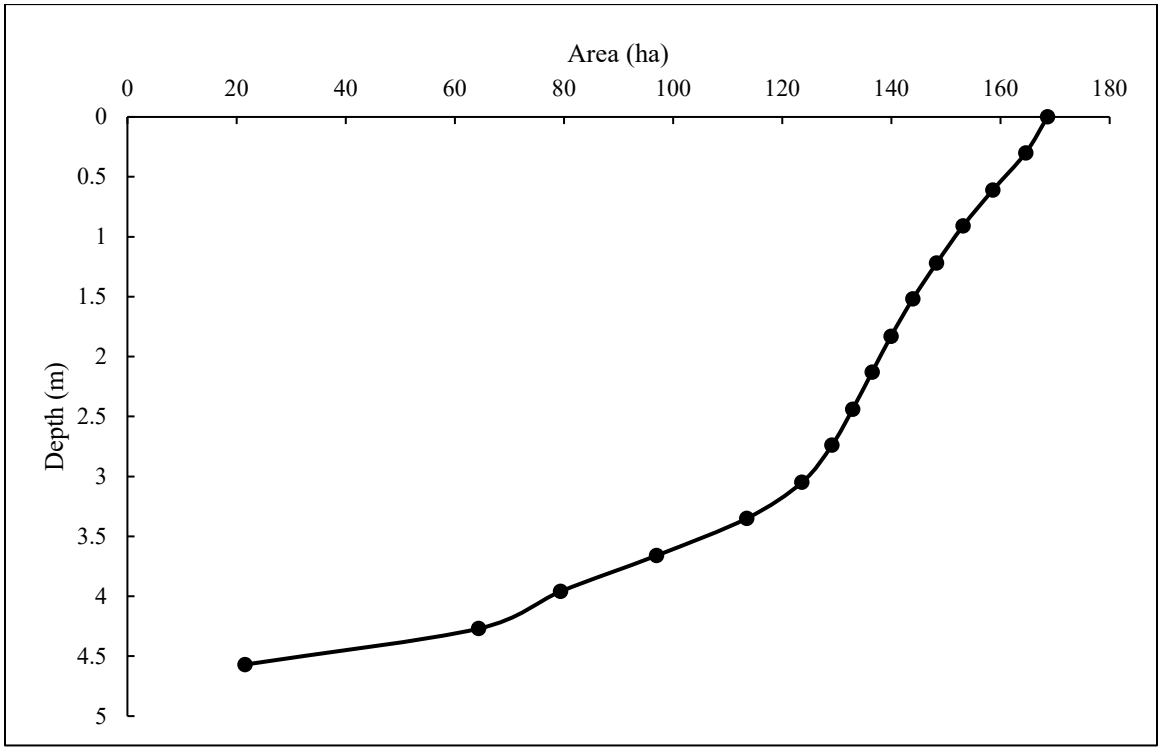

Figure 5.1. Goose Lake Hypsographic Curve

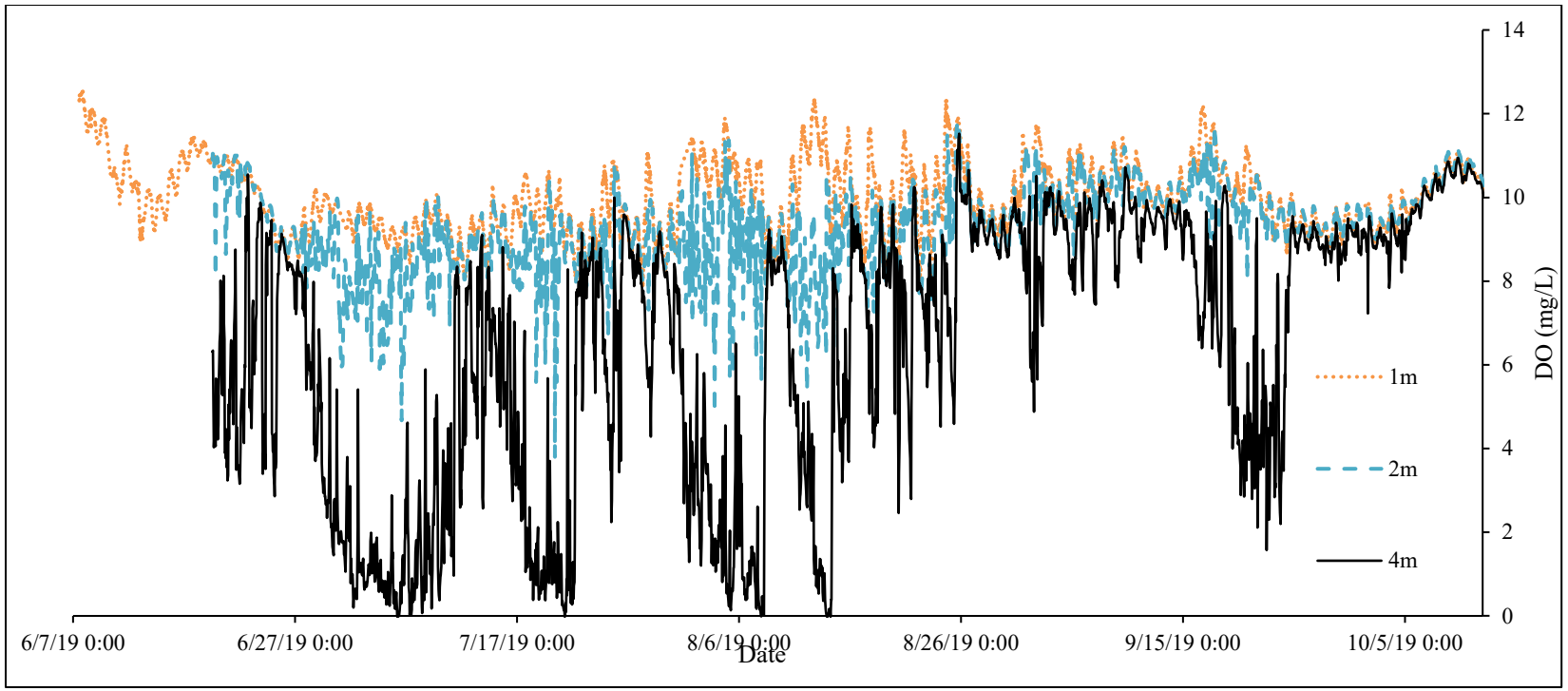

Figure 5.2. Observed 2019 DO Profile

The measured dissolved oxygen profile is shown in Figure 5.2. When the lake is mixed, all depths are at equivalent concentrations, but the 2 and 4 m profiles are drawn down during stratification. For this reason, along with the longest deployment time, the 1 m sonde was assumed to be representative of mixed layer concentrations.

5.2 Metabolism Modeling

The following equation was used to test significance of the cross-correlation:

$$2/\sqrt{n-|k|} \qquad \text{(Minitab LLC 2022) [5.1]}$$

Where n is the number of samples and k is the time lag. This metric corresponds to the Pearson *R* and is listed in the documentation as a rule of thumb for significance. Pearson correlations were then calculated manually to test the *P* values.

There is a slight discrepancy between the cross-correlation coefficient and Pearson correlations for the productivity delta values for identical time lags. This is due to how R handles missing values for the cross-correlations. First, the average of the dLN dt^{-1} for the entire time series is calculated before dates with missing dProductivity dt^{-1} values are thrown out, resulting in a slightly altered correlation. However, the difference in correlation coefficient is at most 0.01, seen in Table 5.1. The significant Pearson correlations had the largest *P* value of 0.033.

Table 5.1. Pearson and Cross-Correlation Comparison

Lag	dNEPdt	dGPPdt	dRdt
	Cross-Correlation		
0	0.225	-	-0.202
-1	-0.342	-0.209	-
	Pearson Correlation		
0	0.221	-	-0.199
-1	-0.332	-0.202	-

A lag of -1 corresponds to the productivity one day after mixing. Values the cross-correlation significance threshold of |Correlation Factor| >= 0.1859 at 0 days and 0.1865 at -1 days were omitted. For the Pearson correlation, values of $p>0.05$ were omitted.

5.3 GLM Modeling

5.3.1 GLM Configuration File

```
&glm_setup
   sim_name = 'Goose_Lake'
   max_layers = 60
   min_layer_vol = 0.025
   min_layer_thick = 0.1
   max_layer_thick = 0.15
   density_model = 1
   ! Uses given daily flow data, and does not interpolate rates between days
   non_avg = .true.
/
&morphometry
   lake_name = 'GooseLake'
   latitude = 46.47073
   longitude = -87.51936
   bsn_len = 2672
   bsn_wid = 1097
   ! In lieu of outflow data, the crest elevation was set to allow the lake to "spill over"
when full
   crest_elev = 372
   bsn_vals = 16
   H = 367.43, 367.73, 368.04, 368.34, 368.65, 368.95, 369.26, 369.56, 369.87, 370.17,
370.48, 370.78, 371.09, 371.39, 371.7, 372
   A = 215369, 643605, 793765, 969877, 1135043, 1236040, 1291021, 1328867,
1364613, 1399331, 1439097, 1482855, 1531220, 1585978, 1646077, 1686000
/
&time
   ! timefmt = 2 utilizes start and end dates, not number of days
   timefmt = 2
   start = '2019-06-08 01:00:00'
   stop = '2019-10-17 23:00:00'
   dt = 3600
   ! Because the analysis was for the summer, the time zone is EDT
   timezone = -4
   ! Not used because timefmt = 2
   num_days = 131
/
&init_profiles
   lake_depth = 4.57
   num_depths = 9
   the_depths = 0.5, 1, 1.5, 2, 2.5, 3, 3.5, 4, 4.5
   the_temps = 19.16, 19.06, 19.13, 19.05, 19.01, 18.89, 18.13, 17.35, 15.41
   ! Because the lake is fresh water, zero salinity was assumed
```

```
  the_sals = 0, 0, 0, 0, 0, 0, 0, 0, 0
/
&meteorology
  met_sw = .true.
  ! Assumes neutral atmospheric stability which is sutable for for seasonal analyses
according to Hipsey et al. (2019)
  atm_stab = 0
  ! This rad mode uses the shortwave radiation data to calculate longwave radiation and
cloud cover
  rad_mode = 3
  ! Uses Yajima and Yamamoto Method
  albedo_mode = 3
  ! Uses Yajima and Yamamoto Method
  cloud_mode = 4
  ! Disables wind sheltering. This was selected since we had on site wind data. The lower
wind factor likely mimics wind sheltering
  fetch_mode = 0
  subdaily = .true.
  meteo_fl = 'nldas_driver_2019_final.csv'
  ! The following factors were all calibration parameters
  wind_factor = 0.711487115
  sw_factor = 1.024595606
  lw_factor = 0.837043668
  at_factor = 0.78724626
  rh_factor = 0.956470433
  ce = 0.001453027
  ch = 0.001473118
  cd = 0.001104396
/
&light
  ! Light mode = 0 uses a single value of Kw for all PAR wavelengths
  light_mode = 0
  ! Kw is a calibration parameter
  Kw = 3.28692823
/
&output
  out_dir = 'output'
  out_fn = 'output'
  nsave = 1
  csv_lake_fname = 'gooselake'
  csv_point_nlevs = 4
  csv_point_fname = 'Temp_'
  csv_point_at = 4, 3, 2, 1
  csv_point_frombot = .false.
  csv_point_nvars = 1
```

```
  csv_point_vars = 'temp'
  csv_ovrflw_fname = 'overflow'
/
&mixing
  surface_mixing = 1
  ! These internal mixing parameters were set to defaults given in Bruce et al. (2018)
  coef_mix_conv = 0.2
  coef_wind_stir = 0.23
  coef_mix_shear = 0.3
  coef_mix_turb = 0.51
  coef_mix_KH = 0.3
  coef_mix_hyp = 0.5
  deep_mixing = 2
  diff = 0
/
&inflow
  num_inflows = 1
  names_of_strms = 'Partridge'
  subm_flag = .false.
  inflow_factor = 1
  inflow_fl = 'PartridgeInflow.csv'
  inflow_varnum = 1
  inflow_vars = 'FLOW'
  ! These streamflow parameters are from the Kinneret example file, as we did not have
streambed data
  coef_inf_entrain = 0
  strm_hf_angle = 85
  strmbd_slope = 4
  strmbd_drag = 0.016
/
```

Table 5.2. GLM Sensitivity Analysis Results

Wind Weight	2019 # M.E.	2019 Longest Strat (hr)	2019 % Strat	GFDL-CM3 4.5 # M.E.	GFDL-CM3 4.5 Longest Strat (hr)	GFDL-CM3 4.5 % Strat	GFDL-CM3 8.5 # M.E.	GFDL-CM3 8.5 Longest Strat (hr)	GFDL-CM3 8.5 % Strat
50	72	324	42.00%	31	468	68.70%	28	1590	74.60%
75	56	33	16.00%	35	435	39.10%	37	300	52.00%
90	35	18	8.20%	27	111	24.70%	34	150	37.30%
110	9	15	2.00%	21	133	12.60%	32	132	26.80%
125	4	9	0.90%	17	42	7.80%	26	114	19.50%
150	0	0	0.00%	14	18	3.80%	22	84	11.40%
K_W Weight	2019 # M.E.	2019 Longest Strat (hr)	2019 % Strat	GFDL-CM3 4.5 # M.E.	GFDL-CM3 4.5 Longest Strat (hr)	GFDL-CM3 4.5 % Strat	GFDL-CM3 8.5 # M.E.	GFDL-CM3 8.5 Longest Strat (hr)	GFDL-CM3 8.5 % Strat
50	21	15	4.50%	27	66	18.80%	33	138	32.80%
75	22	15	5.20%	27	69	18.40%	33	162	33.90%
90	19	15	4.00%	31	69	18.10%	33	138	31.70%
110	22	15	4.50%	25	69	15.40%	34	138	31.00%
125	13	15	3.10%	30	60	14.40%	36	138	31.60%
150	7	15	1.90%	26	57	12.40%	36	138	29.76%
Inflow Weight	2019 # M.E.	2019 Longest Strat (hr)	2019 % Strat	GFDL-CM3 4.5 # M.E.	GFDL-CM3 4.5 Longest Strat (hr)	GFDL-CM3 4.5 % Strat	GFDL-CM3 8.5 # M.E.	GFDL-CM3 8.5 Longest Strat (hr)	GFDL-CM3 8.5 % Strat
50	23	15	5.10%	29	69	16.10%	32	153	31.40%
75	16	15	3.40%	29	69	16.87%	33	138	30.90%
90	21	15	4.10%	27	69	16.80%	35	150	31.90%
110	22	15	5.40%	30	57	15.70%	32	138	31.90%
125	19	15	3.90%	30	69	17.30%	35	141	31.80%
150	24	15	4.70%	32	57	18.10%	36	138	31.70%

5.4 R Code

5.4.1 Calibration Setup

```
# This script set all of the variables necessary for the GLM calibration. It reads in the
field data, calculates the observed Lake Number, and creates empty data frames for other
scripts. The metalimnion depths in Lake Analyzer are changed to allow for a continuous
analysis. This allows a continuous calculation of Lake Number RMSE in the following
script.

# Initialize Session
pacman::p_load(pacman, party, psych, rio, tidyverse,optimization,glmtools,GLM3r,
        Metrics,rLakeAnalyzer,GenSA,processx)
setwd("D:/Masters_Research/Goose_Calibration_Simple_3")
sim_folder <- "D:/Masters_Research/Goose_Calibration_Simple_3"

#simulation path
# Add manually to metalimnion depths: mixed.cutoff = 0
trace(rLakeAnalyzer::ts.lake.number,edit = TRUE)

# Read and convert field observations
TempObs <- read.csv(file = 'observed/ObsTempHour.csv')
dates <- tibble(TempObs$datetime,.rows = 3166)
colnames(dates) <-c("datetime")

#Lake Analyzer Files
bathy <- load.bathy('observed/GooseBathyNew.txt')
wind <- load.ts('observed/Goose_Wind_Hourly_LA_U1.txt')
TempObsLA <- load.ts('observed/ObsTempHour.txt')
#Calculates observed Lake Number
ObsLN <- ts.lake.number(wtr = TempObsLA,
                wnd = wind,
                wnd.height = 1,
                bathy = bathy,
                seasonal = FALSE)

# Replaces negative values with 0
ObsLNClean <- ObsLN$lake.number
ObsLNClean[ObsLNClean < 0] <- 0
ObsTempRMSE <- c(TempObs$wtr_1.0,TempObs$wtr_2.0,
        TempObs$wtr_3.0,TempObs$wtr_4.0)

# Initialized Parameters
temp_RMSE <-list()
LN_RMSE <-list()
i <- 1
```

5.4.2 Simulated Annealing Calibration

```
# This is the cost function for the calibration. It writes the new variables to the .nml file,
runs GLM, and calculates Lake Number and temperature rmse for the model outputs. It
returns the summed NRMSE for both values that are weighted during model setup.
SACalibration <- function(CV, ...) {

 #Edits nml file
 glm_nml <- read_nml('glm3.nml')
 glm_nml <- set_nml(glm_nml, arg_name = 'wind_factor', arg_val = CV[1])
 glm_nml <- set_nml(glm_nml, arg_name = 'sw_factor', arg_val = CV[2])
 glm_nml <- set_nml(glm_nml, arg_name = 'lw_factor', arg_val = CV[3])
 glm_nml <- set_nml(glm_nml, arg_name = 'at_factor', arg_val = CV[4])
 glm_nml <- set_nml(glm_nml, arg_name = 'rh_factor', arg_val = CV[5])
 glm_nml <- set_nml(glm_nml, arg_name = 'ce', arg_val = CV[6])
 glm_nml <- set_nml(glm_nml, arg_name = 'ch', arg_val = CV[7])
 glm_nml <- set_nml(glm_nml, arg_name = 'cd', arg_val = CV[8])
 glm_nml <- set_nml(glm_nml, arg_name = 'Kw', arg_val = CV[9])
 write_nml(glm_nml, file = 'glm3.nml')

 #Runs the GLM Simulation
 run(command = "glm.bat", echo = FALSE)

 # Reads temperature outputs from the netcdf output file
 A <- get_var(file = "output/output.nc", var_name = 'temp',
           reference = "surface", z_out = 1)
 B <- get_var(file = "output/output.nc", var_name = 'temp',
           reference = "surface", z_out = 2)
 C <- get_var(file = "output/output.nc", var_name = 'temp',
           reference = "surface", z_out = 3)
 D <- get_var(file = "output/output.nc", var_name = 'temp',
           reference = "surface", z_out = 4)

 # Converts the modeled temperatures into a suitable format for Lake Analyzer
 TempModel <- tibble(dates, A$temp_1, B$temp_2,
                  C$temp_3, D$temp_4,.rows = 3166)
 colnames(x = TempModel)<-c('datetime','temp_1.0', 'temp_2.0',
                       'temp_3.0', 'temp_4.0')
 write.table(x = TempModel,file = "TempModelFormat.txt", append = FALSE,
          sep = "\t",col.names = TRUE, quote = FALSE)
 TempModelFormat <- load.ts('TempModelFormat.txt')

 #Calculates Lake Number and Rounds to 4 decimal places
 #to remove slightly negative values (ie -1E13)
```

```
 ModelLN <- ts.lake.number(wtr = TempModelFormat,
                           wnd = wind,
                           wnd.height = 1,
                           bathy = bathy,
                           seasonal = FALSE)
ModelLNClean <- ModelLN$lake.number
ModelLNClean[ModelLNClean < 0] <- 0

 #Makes single vector of model temps
 TempModelRMSE <-c(TempModel$temp_1.0,TempModel$temp_2.0,
                   TempModel$temp_3.0,TempModel$temp_4.0)

 #Records RMSE for each iteration
 LN_RMSE_it <- rmse(ObsLNClean,ModelLNClean)
 temp_RMSE_it <- rmse(ObsTempRMSE,TempModelRMSE)

 temp_RMSE[[i]] <<-as.data.frame(list(temp_RMSE_it))
 LN_RMSE[[i]] <<- as.data.frame(list(LN_RMSE_it))
 i <<- i+1
  # Calculates the summed Normalized Root Mean Squared Error

ModelNRMSE <<- rmse(ObsTempRMSE,TempModelRMSE)/mean(ObsTempRMSE)*1
+
   rmse(ObsLNClean,ModelLNClean)/mean(ObsLNClean)*0
 c2 <<- ModelNRMSE
 return(ModelNRMSE)
}
```

5.4.3 Simulated Annealing Call

This function uses a simulated annealing function for model optimization. The lowe and upper parameter bounds of the model are set and then iterate over the previous function. On completion, the script outputs the simulated annealing results as well as the temperature and LN RMSE for each run. These were used to determine the “best” run in absence of a validation dataset.

```
# Sets bounds for simulated annealing function
lower = c(0.7,0.7,0.7,0.7,0.9,.0011,.0011,.0011,0.5)
upper <- c(1.3,1.3,1.3,1.3,1.1,0.0015,0.0016,0.0015,5.0)

#Runs SA function
system.time(
out <<-GenSA(fn = SACalibration,lower = lower,upper = upper,
     control = list(max.call=5000)
     ))

# Outputs parameters
results <- out[c("value","par","counts","trace.mat")]
temp_RMSE_List <- rbind.data.frame(temp_RMSE)
LN_RMSE_List <- rbind.data.frame(LN_RMSE)
write.csv(LN_RMSE_List,"logs/LN_RMSE_PC3_6_2.csv")
write.csv(temp_RMSE_List,"logs/temp_RMSE_PC3_6_2.csv")
capture.output(out,file = 'logs/results_PC3_6_2.csv')
```

5.4.4 2019 Mixing Analysis

```
# This code read in the GLM inputs and model outputs to calculate the Lake Number
time series for the model. Run length encoding was then used to determine the number of
mixing events and stratification extent for the study period. The data processing was
specific to this dataset and would need to be modified for different length datasets.

# Initialize Session
pacman::p_load(pacman, party, psych, rio, tidyverse,optimization,glmtools,GLM3r,
          Metrics,rLakeAnalyzer,GenSA,processx,lubridate)
# Add manually to metalimnion depths: mixed.cutoff = 0
trace(rLakeAnalyzer::ts.lake.number,edit = TRUE)

# This reads from the nldas_driver from the GLM model
setwd("C:/Users/breus/Documents/Masters_Research/Goose_Calibration_Final")
driver = 'nldas_driver_2019_final.csv'
path_out = 'LN/2019 Final'

# This is used to scale the wind speed for LA
wind_scalar = 1

rle_out = 'rle.csv'
LN_out = 'LNClean.csv'
Temp_avg_out = 'Avg_Layer_Temp.csv'

# Reads water temperature outputs from the .nc file
A <- get_var(file = "output/output.nc", var_name = 'temp',
          reference = "surface", z_out = 1)
B <- get_var(file = "output/output.nc", var_name = 'temp',
          reference = "surface", z_out = 2)
C <- get_var(file = "output/output.nc", var_name = 'temp',
          reference = "surface", z_out = 3)
D <- get_var(file = "output/output.nc", var_name = 'temp',
          reference = "surface", z_out = 4)
#Combines temperature data into a single dataframe and removes dates through
# 6/8 0100.

Temperature <- data.frame('datetime' = A$DateTime,"temp_1" = A$temp_1,
                    'temp_2' = B$temp_2,'temp_3' = C$temp_3, 'temp_4' = D$temp_4)

# Depth Temperature Averages
one_meter_avg <- mean(Temperature$temp_1)
two_meter_avg <- mean(Temperature$temp_2)
three_meter_avg <- mean(Temperature$temp_3)
four_meter_avg <- mean(Temperature$temp_4)
Temp_avg <- data.frame('1m' = one_meter_avg, '2m' = two_meter_avg,
```

```
                '3m' = three_meter_avg, '4m' = four_meter_avg)

# Averages hourly outputs to 3 hours which matches the available wind data
# https://community.rstudio.com/t/how-to-take-the-average-of-every-3-rows/101338
GroupLabels <- 0:(nrow(Temperature)-1) %/% 3
Temperature$Group <- GroupLabels
Temp3hr <- Temperature %>% group_by(Group) %>% summarize(Avg = data.frame(
  'datetime' = mean(datetime),'wtr_1.0' = mean(temp_1), 'wtr_2.0' = mean(temp_2),
  'wtr_3.0' = mean(temp_3), 'wtr_4.0' = mean(temp_4)))

# Writes the temp data into a Lake Analyzer compatable format
Temp_LA <- data.frame('datetime' = Temp3hr$Avg$datetime,
'wtr_1.0'= Temp3hr$Avg$wtr_1.0,'wtr_2.0'= Temp3hr$Avg$wtr_2.0,
'wtr_3.0'= Temp3hr$Avg$wtr_3.0,'wtr_4.0'= Temp3hr$Avg$wtr_4.0)

write.table(Temp_LA,'LN/Model Temp 3hr.txt', sep = "\t",
          col.names = TRUE,row.names = FALSE,quote = FALSE)

# Reads the wind data from the nldas_driver file and averages to 3 hr, writes to LA
wind_GLM = read.csv(driver)
wind_GLM <- wind_GLM[2:3167,]
GroupLabelsWind <- 0:(nrow(wind_GLM)-1) %/% 3
wind_GLM$Group <- GroupLabelsWind
names(wind_GLM)[names(wind_GLM) == 'time'] <- 'datetime'
wind_GLM$datetime <- ymd_hm(wind_GLM$datetime)
Wind3hr <- wind_GLM %>% group_by(Group) %>% summarize(Avg = data.frame(
  'datetime' = mean(datetime),'WindSpeed' = mean(WindSpeed)))
wind_LA = data.frame('dateTime' = Wind3hr$Avg$datetime,
                  'windSpeed' = Wind3hr$Avg$WindSpeed)
write.table(wind_LA,'LN/Model Wind 3hr U10.txt', sep = "\t", col.names = TRUE,
          row.names = FALSE,quote = FALSE)

#Lake Analyzer Files
bathy <- load.bathy('LN/GooseBathyNew.txt')
wind <- load.ts('LN/Model Wind 3hr U10.txt')

TempObsLA <- load.ts('LN/Model Temp 3hr.txt')
#Calculates observed Lake Number
ObsLN <- ts.lake.number(wtr = TempObsLA,
                        wnd = wind,
                        wnd.height = 10,
                        bathy = bathy,
                        seasonal = FALSE)

# Replaces negative values with 0
```

```
ObsLNClean <- ObsLN$lake.number
ObsLNClean[ObsLNClean < 0] <- 0

# True is for periods of stratification where LN >1
# Run Length Encoding to determine when LN > 1
a <- rle(ObsLNClean > 1)
a_comb <- data.frame(a$lengths,a$values)
#Writes outputs to files
write.csv(a_comb,paste(path_out,rle_out,sep = ''))
write.csv(ObsLNClean,paste(path_out,LN_out,sep = ''))
write.csv(Temp_avg,paste(path_out,Temp_avg_out,sep = ''))
```

5.4.5 Future Scenario Mixing Analysis

```
# This script automatically ran all weights for the sensitivity analysis. It used the GLM
inputs which were consistent between runs and each model output to calculate the Lake
Number time series. Then stratification extent and mixing periods were calculated using
run length encoding. The data processing was specific to this dataset and would need to
be modified for different length datasets.

# Initialize Session
pacman::p_load(pacman, party, psych, rio, tidyverse,optimization,glmtools,GLM3r,
          Metrics,rLakeAnalyzer,GenSA,processx,lubridate)
# Add manually to metalimnion depths: mixed.cutoff = 0
trace(rLakeAnalyzer::ts.lake.number,edit = TRUE)

# This reads from the 3hour nldas_driver for the 3 hour windspeed

# File name components for loop
rle_out = 'rle.csv'
LN_out = 'LNClean.csv'
Temp_avg_out = 'Avg_Layer_Temp.csv'

# The loop iterates for each parameter weight
scalars <- c(50,75,90,110,125,150)
for (i in scalars){

wd <-
'C:/Users/breus/Documents/Masters_Research/Climate_Spreadsheet/Sensitivity_Analyse
s/Wind_Sensitivity/GFDL-CM3/RCP8_5/GLM'
pout <-  'LN/GFDL_CM3 8_5 Wnd'

setwd(paste(wd,i,sep = ''))
# Reads in the GLM model inputs. These remain constant between sensitivity analyses
# with the exception of wind, which is scaled in the loop.
driver = 'nldas_driver_GFDL-CM3_8_5.csv'
path_out = paste(pout,i,sep = '')

# For the wind sensitivity analyses, the wind data must be scaled for Lake Analyzer
# For all other analyses, wind scalar = 1
wind_scalar = i/100

# Reads water temperature outputs from the .nc file
A <- get_var(file = "output/output.nc", var_name = 'temp',
          reference = "surface", z_out = 1)
B <- get_var(file = "output/output.nc", var_name = 'temp',
          reference = "surface", z_out = 2)
C <- get_var(file = "output/output.nc", var_name = 'temp',
```

```
        reference = "surface", z_out = 3)
D <- get_var(file = "output/output.nc", var_name = 'temp',
        reference = "surface", z_out = 4)

#Combines temperature data into a single dataframe and removes dates through
# 6/8 0100.

Temperature <- data.frame('datetime' = A$DateTime,"temp_1" = A$temp_1,
                  'temp_2' = B$temp_2,'temp_3' = C$temp_3, 'temp_4' = D$temp_4)
Temperature <- Temperature[167:3333,]

# Depth Temperature Averages
one_meter_avg <- mean(Temperature$temp_1)
two_meter_avg <- mean(Temperature$temp_2)
three_meter_avg <- mean(Temperature$temp_3)
four_meter_avg <- mean(Temperature$temp_4)

Temp_avg <- data.frame('1m' = one_meter_avg, '2m' = two_meter_avg,
                '3m' = three_meter_avg, '4m' = four_meter_avg)

# Averages hourly outputs to 3 hours which matches the available wind data
# https://community.rstudio.com/t/how-to-take-the-average-of-every-3-rows/101338
GroupLabels <- 0:(nrow(Temperature)-1) %/% 3
Temperature$Group <- GroupLabels
Temp3hr <- Temperature %>% group_by(Group) %>% summarize(Avg = data.frame(
  'datetime' = mean(datetime),'wtr_1.0' = mean(temp_1), 'wtr_2.0' = mean(temp_2),
  'wtr_3.0' = mean(temp_3), 'wtr_4.0' = mean(temp_4)))

# Writes the temp data into a Lake Analyzer compatable format
Temp_LA <- data.frame('datetime' = Temp3hr$Avg$datetime,
'wtr_1.0'= Temp3hr$Avg$wtr_1.0,'wtr_2.0'= Temp3hr$Avg$wtr_2.0,
'wtr_3.0'= Temp3hr$Avg$wtr_3.0,'wtr_4.0'= Temp3hr$Avg$wtr_4.0)

write.table(Temp_LA,'LN/Model Temp 3hr.txt', sep = "\t",
          col.names = TRUE,row.names = FALSE,quote = FALSE)

# Reads the wind data from the nldas_driver file and writes to LA
wind_GLM_raw = read.csv(driver)

# This pulls the time data from the GLM output file since it is already in the right format
wind_GLM <- data.frame('datetime' = wind_GLM_raw$time[57:1112],
                  'WindSpeed' = wind_GLM_raw$WindSpeed[57:1112]*wind_scalar)
wind_LA = data.frame('dateTime' = wind_GLM$datetime,
                'windSpeed' = wind_GLM$WindSpeed)
write.table(wind_LA,'LN/Model Wind 3hr U10.txt', sep = "\t", col.names = TRUE,
```

```
        row.names = FALSE,quote = FALSE)

#Lake Analyzer Files
bathy <- load.bathy('LN/GooseBathyNew.txt')
wind <- load.ts('LN/Model Wind 3hr U10.txt')
TempObsLA <- load.ts('LN/Model Temp 3hr.txt')

#Calculates observed Lake Number
ObsLN <- ts.lake.number(wtr = TempObsLA,
                        wnd = wind,
                        wnd.height = 10,
                        bathy = bathy,
                        seasonal = FALSE)

# Replaces negative values with 0
ObsLNClean <- ObsLN$lake.number
ObsLNClean[ObsLNClean < 0] <- 0

# True is for periods of stratification where LN >1
# Run Length Encoding to determine when LN > 1
a <- rle(ObsLNClean > 1)
a_comb <- data.frame(a$lengths,a$values)

#Writes outputs to files
write.csv(a_comb,paste(path_out,rle_out,sep = ''))
write.csv(ObsLNClean,paste(path_out,LN_out,sep = ''))
write.csv(Temp_avg,paste(path_out,Temp_avg_out,sep = ''))
}
```